iScience

CellPress
OPEN ACCESS

Article

Immunogenic tumor cell death promotes dendritic cell migration and inhibits tumor growth via enhanced T cell immunity

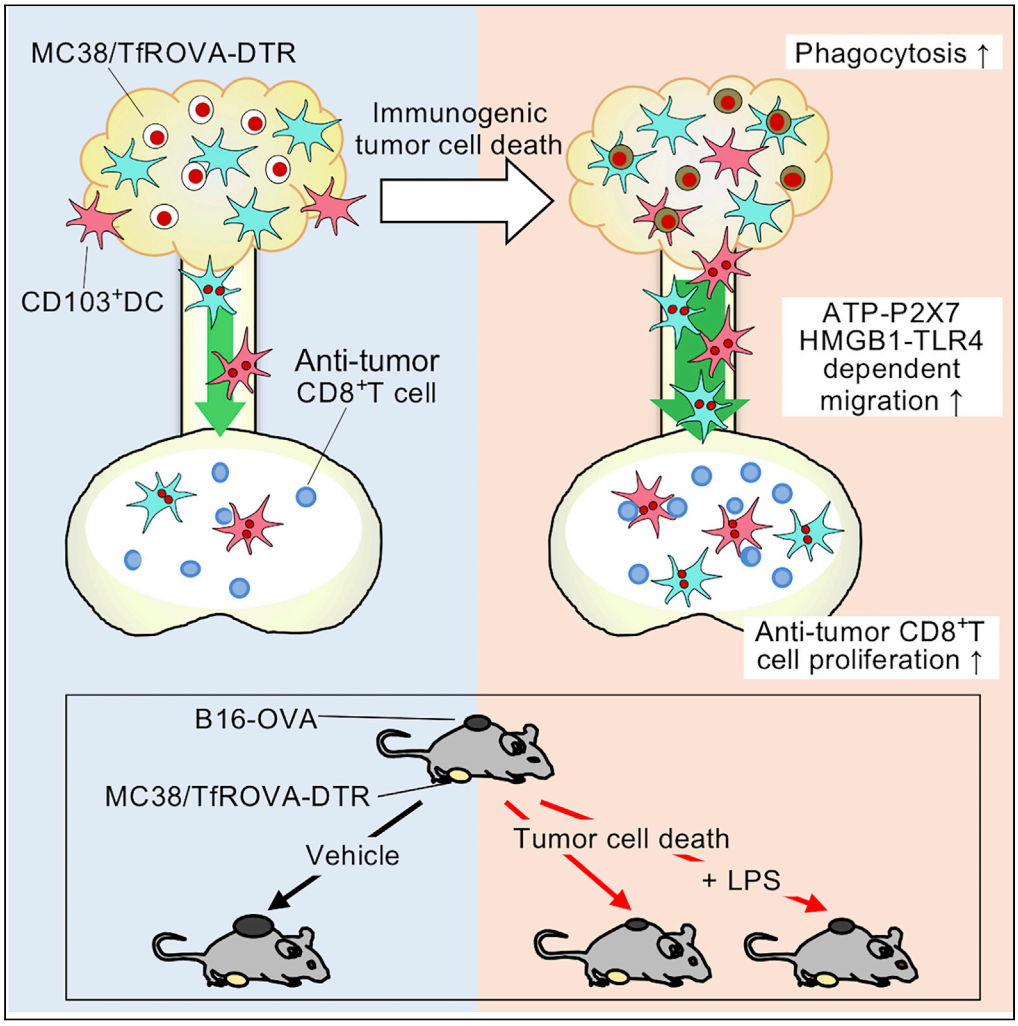

Taiki Moriya, Kurumi Kitagawa, Yuuki Hayakawa, ..., Yutaka Kusumoto, Tatyana Chtanova, Michio Tomura

michio.tomura@gmail.com

Highlights

Immunogenic cell death (ICD) promotes egress of tumor-infiltrating (Ti)-DCs to dLNs

ICD induced Ti-DC migration to dLNs utilizes P2X7R and HMGB1 signaling pathways

LPS treatment attenuates the anti-tumor effects of ICD

$CD103^+$ DCs are required at the time of ICD for suppression of secondary tumor growth

Moriya et al., iScience 24, 102424
May 21, 2021
https://doi.org/10.1016/j.isci.2021.102424

iScience

CellPress
OPEN ACCESS

Article

Immunogenic tumor cell death promotes dendritic cell migration and inhibits tumor growth via enhanced T cell immunity

Taiki Moriya,[1] Kurumi Kitagawa,[1] Yuuki Hayakawa,[1] Hiroaki Hemmi,[2] Tsuneyasu Kaisho,[2] Satoshi Ueha,[3] Ryoyo Ikebuchi,[1,4] Ippei Yasuda,[1] Yasutaka Nakanishi,[1] Tetsuya Honda,[5] Koji Matsushima,[3] Kenji Kabashima,[5] Mizuki Ueda,[1] Yutaka Kusumoto,[1] Tatyana Chtanova,[6,7] and Michio Tomura[1,8,*]

SUMMARY

Immunogenic tumor cell death enhances anti-tumor immunity. However, the mechanisms underlying this effect are incompletely understood. We established a system to induce tumor cell death *in situ* and investigated its effect on dendritic cell (DC) migration and T cell responses using intravital photolabeling in mice expressing KikGR photoconvertible protein. We demonstrate that tumor cell death induces phagocytosis of tumor cells by tumor-infiltrating (Ti)-DCs, and HMGB1-TLR4 and ATP-P2X7 receptor signaling-dependent Ti-DC emigration to draining lymph nodes (dLNs). This led to an increase in anti-tumor CD8$^+$ T cells of memory precursor effector phenotype and secondary tumor growth inhibition in a CD103$^+$ DC-dependent manner. However, combining tumor cell death induction with lipopolysaccharide treatment stimulated Ti-DC maturation and emigration to dLNs but did not improve tumor immunity. Thus, immunogenic tumor cell death enhances tumor immunity by increasing Ti-DC migration to dLNs where they promote anti-tumor T cell responses and tumor growth inhibition.

INTRODUCTION

Chemotherapy and radiation therapy induce tumor cell death (Galluzzi et al., 2017; Montico et al., 2018; Zitvogel et al., 2008) and stimulate anti-tumor immunity through immunogenic cell death (ICD) and increased supply of tumor antigens. In ICD, damage-associated molecular patterns (DAMPs) molecules, calreticulin (CRT), heat shock protein (HSP)-70, and HSP-90 are expressed on the plasma membrane of dying tumor cells, and adenosine triphosphate (ATP) and high-mobility group box (HMGB) 1 are released from dying tumor cells. ATP released from oxaliplatin-killed tumor cells stimulates dendritic cells (DCs) in tumors via P2X7 receptor (P2X7R) and enhances systemic anti-tumor immunity induced in draining lymph nodes (dLNs) (Ghiringhelli et al., 2009). Similarly, HMGB1 released from anthracycline-treated dying tumor cells has robust adjuvant-like effects achieved by stimulating toll-like receptor (TLR) 4 and inducing maturation and antigen processing by DCs (Fucikova et al., 2011; Hato et al., 2014). Furthermore, injection of doxorubicin-killed tumor cells or intra-tumoral injection of doxorubicin suppressed tumor growth *in vivo* (Casares et al., 2005). In these cases, induction of anti-tumor CD8$^+$ T cells by DCs that migrated from tumor sites to dLNs is crucial for anti-tumor immunity (Durgeau et al., 2018). Both direct and indirect presentation pathways have been reported to play a substantial role in CD8$^+$ T cell priming in dLNs. Direct priming involves phagocytosis of spontaneously generated dying tumor cells by tumor-infiltrating (Ti)-DCs, followed by migration to dLNs and subsequent presentation of tumor antigens to CD8$^+$ T cells (Abbas et al., 2015; Sadozai et al., 2017). Migratory CD103$^+$ DCs have been reported to play a critical role in inducing anti-tumor CD8$^+$ T cell immune responses (Roberts et al., 2016; Salmon et al., 2016) by shuttling tumor antigens to dLNs and directly presenting antigen-derived peptides with major histocompatibility complex (MHC) class I molecules to stimulate CD8$^+$ T cells. On the other hand, indirect priming involves CD8α^+ lymph node-resident DCs (LNDCs), which receive tumor antigens from migratory CD103$^+$ and CD103$^-$ CD11b$^+$ DCs (cDC2) (Roberts et al., 2016) and then present tumor antigens to CD8$^+$ T cells. Thus, recruitment to tumors and subsequent emigration of immune cells, especially CD103$^+$ and CD103$^-$ Ti-DCs, from tumors to dLNs are crucial steps for effective anti-tumor immunity. CD103$^-$ DCs (cDC2) can also promote tumor growth regression by inducing Th17 responses (Laoui et al., 2016). Therefore, both CD103$^+$ Ti-DCs and CD103$^-$ Ti-DCs

[1]Laboratory of Immunology, Faculty of Pharmacy, Osaka Ohtani University, Tondabayashi, Osaka 584-8540, Japan

[2]Department of Immunology, Institute of Advanced Medicine, Wakayama Medical University, Graduate school of Medicine, Wakayama, Wakayama 641-8509, Japan

[3]Division of Molecular Regulation of Inflammatory and Immune Diseases, Research Institute for Biomedical Sciences, Tokyo University of Science, Noda City Chiba 278-0022, Japan

[4]Research Fellow of Japan Society for the Promotion of Science, Tokyo, Japan

[5]Department of Dermatology, Kyoto University, Graduate School of Medicine, Sakyou-ku, Kyoto 606-8507, Japan

[6]Immunology Theme, Garvan Institute of Medical Research, Darlinghurst, NSW 2010, Australia

[7]School of Biotechnology and Biomolecular Sciences, Faculty of Science, University of New South Wales Sydney, Kensington, NSW 2033 Australia

[8]Lead contact

*Correspondence: michio.tomura@gmail.com

https://doi.org/10.1016/j.isci.2021.102424

have important roles in anti-tumor immunity and possess different functions and need to be analyzed separately.

Notably, other DC subsets such as $CD11c^{+}CD11b^{+}Ly6C^{hi}$ monocyte-derived inflammatory dendritic cells (MoDCs) act *in situ* (within tumors) to mediate ICD-induced inhibition of primary tumor growth (Ma et al., 2013). ATP released from killed tumor cells induces intratumoral recruitment and differentiation of MoDCs. They then phagocytose dying tumor cells and promote antigen presentation within tumors.

Adjuvants, such as TLR ligands, CpG oligodeoxynucleotide (Pashenkov et al., 2006), and lipopolysaccharide (LPS) (Shetab Boushehri et al., 2018) have been utilized to enhance anti-tumor immunity. However, given that TLR ligand stimulation induces DC maturation, it is unclear what effect TLR ligands in combination with ICD have on maturation and migration of Ti-DCs' subsequent stimulation of anti-tumor T cell responses.

Tumor-infiltrating effector $CD8^{+}$ T cells can be subdivided into 3 populations based on expression of cell surface molecules KLRG1 and CD127. $KLRG1^{-}$ $CD127^{+}$ memory precursor effector cells (MPECs) possess similar effector functions to $KLRG1^{+}$ $CD127^{-}$ short-lived effector cells (SLECs), but persist for longer than SLECs. Thus, MPECs would provide a more sustained anti-tumor response (Joshi et al., 2007). In addition, $KLRG1^{+}$ $CD127^{+}$ double-positive effector cells (DPECs) have been reported to provide strong anti-tumor immunity and promote tumor growth control in B16 melanoma (Kobayashi et al., 2015). Consistent with an important role for DPECs, treatment with agonistic antibody against 4-1BB, a co-stimulatory molecule expressed on activated T cells, led to increased DPECs and enhanced anti-tumor immunity (Kobayashi et al., 2015). Thus, elucidating the effect of ICD on generation of effector and memory $CD8^{+}$ T cells is crucial to understanding how ICD affects anti-tumor immunity.

Despite the importance of Ti-DC migration for the anti-tumor response, it is not clear how this migration is affected by ICD. Specifically, we currently lack quantitative and qualitative information about influx and retention of $CD103^{+}$ and $CD103^{-}$ Ti-DCs within tumors and their emigration to dLN both in the steady state and following ICD *in situ*. Furthermore, it is unknown how molecules secreted by immunogenic dying tumor cells regulate migration and function of $CD103^{+}$ and $CD103^{-}$ Ti-DCs. Understanding how ICD regulates endogenous $CD103^{+}$ and $CD103^{-}$ Ti-DC and $CD8^{+}$ T cell migration on its own and in combination with adjuvants will provide insights into the mechanism of ICD-elicited anti-tumor immunity.

One of the confounding factors in uncovering the effect of ICD on the immune response is that chemotherapeutic drugs are immunosuppressive making it difficult to delineate the effects of ICD and chemotherapy on hematopoietic cells. To circumvent this limitation, we established a system where adenocarcinoma cells were engineered to express human diphtheria toxin (DT) receptor (DTR) (Saito et al., 2001) making it possible to induce ICD and generate tumor cell antigens *in situ* while avoiding immunosuppressive effects of chemotherapy. To monitor immune cell emigration from tumors quantitatively, we utilized mice expressing a photoconvertible protein KikGR to label and track tumor-infiltrating cells (Tomura et al., 2014; Torcellan et al., 2017). Here we implanted modified adenocarcinoma cells in mice expressing a photoconvertible protein and elucidated the effect of ICD on endogenous Ti-DC dynamics in tumor and migration and function, as well as tumor antigen-specific T cell response and anti-tumor immunity.

RESULTS

Immunogenic tumor cell death induction *in situ* enhances Ti-DC phagocytosis of dying tumor cells

Although immunization with killed tumor cells can enhance host tumor immunity (Apetoh et al., 2007; Asano et al., 2011), how this process affects endogenous Ti-DC dynamics and subsequent anti-tumor immune response is not known due to the difficulty in analyzing these cells *in situ* in intact tumors. To address this issue, we established a model for inducing and visualizing tumor cell death. We generated colon adenocarcinoma MC38 cell line expressing (1) membrane-bound ovalbumin by fusing it to transferrin receptor (TfROVA) (Teasdale et al., 1992), (2) DTR for tumor cell death induction (Saito et al., 2001), and (3) nuclei-localized red fluorescent protein tandem Keima (Kogure et al., 2006) for visualizing tumor cell nuclei (MC38/TfROVA-DTR). First, we examined whether DT-induced cell death demonstrated typical signs of ICD. Cultured MC38/TfROVA-DTR cells were treated with DT to induce cell death. We then analyzed the supernatants and detected increased CRT expression as well as higher concentration of HMGB1 and

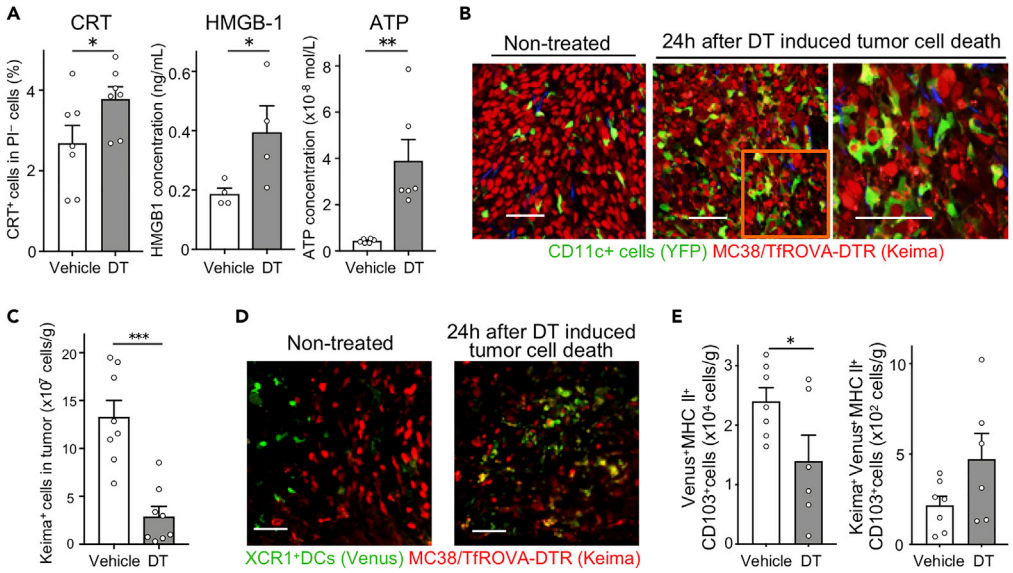

Figure 1. Induction of immunogenic tumor cell death enhances Ti-DC phagocytosis

(A) MC38/TfROVA-DTR tumors were treated with DT or vehicle. Proportions of CRT^+PI^- cells (left) and concentration of HMGB-1 (center) and ATP (right) in culture supplement are shown. Bar graphs show means ± SEM of pooled data from two independent experiments (CRT: n = 7, HMGB-1: n = 4, ATP: n = 6). *p < 0.05, **p < 0.01 (Mann-Whitney U test).

(B and C) MC38/TfROVA-DTR tumor-bearing CD11c-YFP mice 24 h after DT or vehicle treatment. Two-photon microscopic images of tumors (B); the number of $Keima^+CD45^-$ cells in tumors was calculated using data obtained from flow cytometric analysis (C). Scale bars, 50 μm. Bar graph shows means ± SEM of pooled data from two independent experiments (n = 8). ***p < 0.001 (Mann-Whitney U test).

(D and E) MC38/TfROVA-DTR tumor-bearing XCR1-Venus mice 24 h after DT or vehicle treatment. Fluorescence microscopic images (D), the number of $Venus^+$ $MHC\ II^+$ $CD103^+$ cells in tumors (left), and $Keima^+$ $Venus^+$ $MHC\ II^+$ $CD103^+$ cells in tumors (right) (E). Scale bars, 50 μm, Bar graphs show means ± SEM of pooled data from two independent experiments (n = 6–7). *p < 0.05, ***p < 0.001 (Mann-Whitney U test).

ATP (Figures 1A and S1A). Similarly, DT treatment increased ATP concentration in cell culture supernatants from DTR-expressing NIH/3T3 and 3LL cell lines (Figure S1B). These results indicate that DT-induced cell death is ICD.

Next, we determined whether DT injection induces death of MC38/TfROVA-DTR cells and phagocytosis of dying tumor cells by tumor-infiltrating immune cells *in vivo*. MC38/TfROVA-DTR cells were inoculated in CD11c-YFP reporter mice in which $CD11c^+$ cells express YFP (Lindquist et al., 2004). Five days following tumor cell inoculation, YFP^+ cells were interspersed among $Keima^+$ tumor cells, but only a few YFP^+ cells phagocytosed tumor cells (Figure 1B). However, 24 h after induction of ICD by intraperitoneal injection of DT, the number of live tumor cells in treated tumors decreased to approximately 25% of the starting number (Figure 1C). Furthermore, we observed fragmented $Keima^+$ nuclei, some of which were contained inside of YFP^+ cells suggesting that tumor-infiltrating immune cells phagocytosed tumor cell debris (Figure 1B). As CD11c can be expressed by several subsets of myeloid cells in tumors (Ma et al., 2013), we identified YFP^+ cell subsets in tumors in CD11c-YFP mice. YFP^+ cells in tumors consisted of approximately 50% MoDCs, 25% $CD11c^+$ macrophages, less than 10% $CD103^-$ Ti-DCs, and less than 1% $CD103^+$ Ti-DCs (Figure S2A).

It is thought that $CD103^+$ Ti-DCs phagocytose dying tumor cells and mature and migrate to dLNs (Böttcher and Reis e Sousa, 2018). Previous studies reported that $CD103^+$ DCs are localized at edge of the tumor mass (Broz et al., 2014); however it is unclear where $CD103^+$ DCs acquire tumor antigen. To shed light on this and demonstrate that ICD increases phagocytosis by $CD103^+$ DCs in tumors, we analyzed the effect of ICD on $CD103^+$ DC localization and phagocytosis using XCR1-Venus reporter mice that express Venus fluorescent protein selectively in $CD103^+$ DCs and $CD8\alpha^+$ LNDCs (Yamazaki et al., 2013). Consistent with previous reports (Broz et al., 2014), 5 days after MC38/TfROVA-DTR inoculation, we observed $Venus^+$ cells only at the edge of the tumor (Figure 1D). However, 24 h after ICD induction, we observed $Venus^+$ cells containing fragmented $Keima^+$ nuclei that have infiltrated the tumor mass (Figure 1D). Furthermore, $Venus^+$

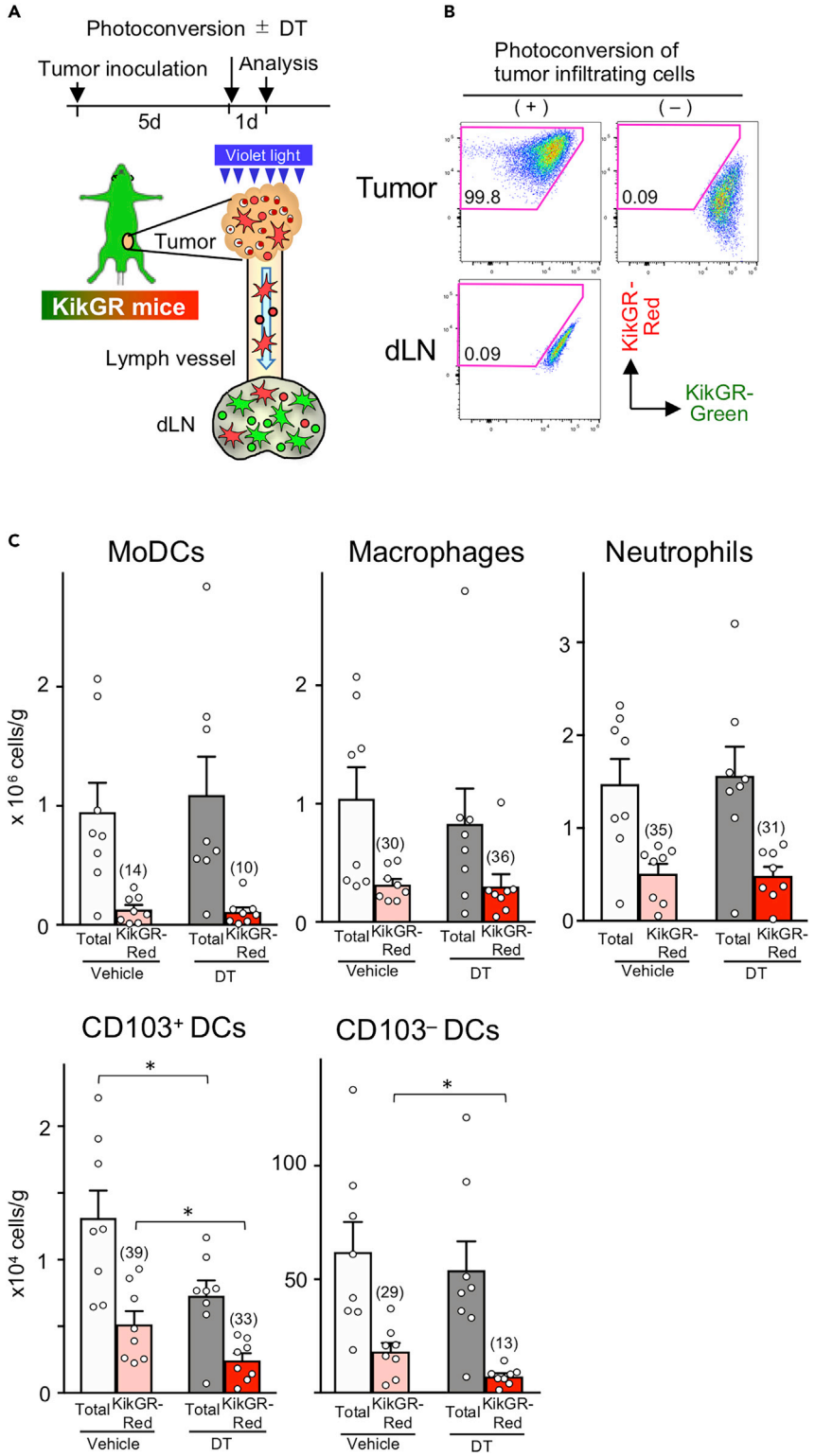

Figure 2. Immunogenic tumor cell death decreases the number of CD103$^+$ and CD103$^-$ Ti-DCs retained in tumors

(A) Experimental setup for the analysis of tumor DC turnover and migration to dLNs. Tumor-infiltrating KikGR$^+$ cells were photoconverted by exposure to violet light, and at the same time, tumor cell death was induced by DT administration. Cells in tumors and dLNs were analyzed 24 h later.

Figure 2. *Continued*

(B) KikGR cells were detected in photoconverted and non-photocoverted tumors and inguinal dLNs in KikGR mice immediately after photoconversion. Data are representative of at least three independent experiments.

(C) Number of total and KikGR-Red MoDCs, F4/80^{+}CD11c^{+} macrophage, neutrophil, CD103^{-} Ti-DCs, CD103^{+} Ti-DCs, and CD103^{-} DCs in MC38/TfROVA-DTR tumors in KikGR mice 24 h following photoconversion and vehicle or DT treatment. Bar graph shows means ± SEM of pooled data from two independent experiments (n = 8). Numbers in bar graphs indicate frequencies of KikGR-Red population (%) in each subset. *p < 0.05 (Mann-Whitney U test).

cells were decreased, whereas Keima^{+} Venus^{+} cells tended to increase (Figures 1E and S2C). Thus, these results suggest that ICD induces CD103^{+} Ti-DC penetration of tumors, which may promote DC phagocytosis of dying tumor cells.

Immunogenic tumor cell death induction decreases the number of tumor-remaining migratory Ti-DCs

To analyze Ti-DC kinetics in tumors, we utilized photoconvertible KikGR mice. KikGR protein is initially green (KikGR-Green), but can be irreversibly photoconverted to red (KikGR-Red) by exposure to violet light (Tomura et al., 2014). Thus, after photolabeling cells within tumors and analyzing cellular content at specific time points by flow cytometry, we can distinguish cells that have been retained in tumors following photoconversion from cells that recently entered tumors and track cell migration of photoconverted cells to other anatomical sites. Tumor-infiltrating cells in KikGR mice inoculated with MC38/TfROVA-DTR cells 5 days earlier were photoconverted and the number of photoconverted, and non-photoconverted cells per gram of tumor was assessed 24 h later (Figures 2A and 2B).

In the absence of ICD, 24 h after photoconversion, the proportion of KikGR-Red myeloid cells retained in tumors varied by subsets: MoDCs (14%), F4/80^{+}CD11c^{+} macrophage (30%), neutrophil (35%), CD103^{-}Ti-DCs (29%), and CD103^{+} Ti-DCs (39%) (Figure 2C and S3). This indicates that a large proportion of cells in each subset entered the tumors during the previous 24 h. When ICD was induced and tumors were photoconverted, the number of total and KikGR-Red tumors retained MoDCs, F4/80^{+}CD11c^{+} macrophages, and neutrophils was not altered, suggesting that ICD had limited effect on the kinetics of these subsets (Figure 2C). On the other hand, although ICD did not decrease the total number of CD103^{-} DCs, it did lead to a reduction in the number of KikGR-Red CD103^{-} DCs. Furthermore, ICD decreased both the number of total and KikGR-Red CD103^{+} Ti-DCs (Figure 2C). These results suggest that ICD induction has a greater impact on the kinetics of Ti-DCs than other immune subsets.

Immunogenic tumor cell death stimulates Ti-DC migration to dLN

We next examined whether ICD can enhance Ti-DC migration to dLN. As shown in Figure 2B, no KikGR-Red cells were detected in inguinal dLN immediately after photoconversion, indicating that photoconversion was restricted to the tumor mass. Twenty-four hours following photoconversion, we detected KikGR-Red cells among migratory DCs (CD11c^{int} MHC class II^{high}), but not among LNDCs (CD11c^{high} MHC class II^{int}) (Figures 3A and S4A).

To confirm that Ti-DCs that migrated to dLNs have the capacity to induce tumor antigen-specific T cell responses, KikGR-Red and KikGR-Green migratory DCs and LNDCs were purified from dLNs and mixed with OVA-specific OT-I T cells that were labeled with CellTrace Violet to track cell division. We found that KikGR-Red migratory DCs strongly induced proliferation of tumor-specific T cells when compared with KikGR-Green migratory DCs. LNDCs did not induce T cell proliferation (Figure 3B). These results suggest that migratory Ti-DCs are the main tumor-antigen-presenting DC subset in this model.

As migratory DCs in LNs consist of CD103^{+}, CD103^{-}, and CD326^{+} (classified as Langerhans cells [Henri et al., 2010]) subsets (Tomura et al., 2014), we analyzed the expression of these markers by DCs 24 h after photoconversion to identify which subsets emigrated from photoconverted tumors. Our analysis detected KikGR-Red cells in all migratory DC subsets, and CD103^{-} DCs were the major subset of migratory Ti-DCs (Figure S4B). The highest number of tumor-emigrating DCs in all subsets was detected in dLNs at 48 h following tumor photoconversion (Figure 3C). Notably, induction of ICD substantially increased the number of KikGR-Red Ti-DCs of each phenotype found in dLNs after 24 h. To confirm that this effect is not restricted to a specific cancer model, we demonstrated that DT-induced cell death increased CD103^{+} and CD103^{-} Ti-DC migration to dLNs from 3LL-DTR tumor in KikGR mice 24 h following photoconversion

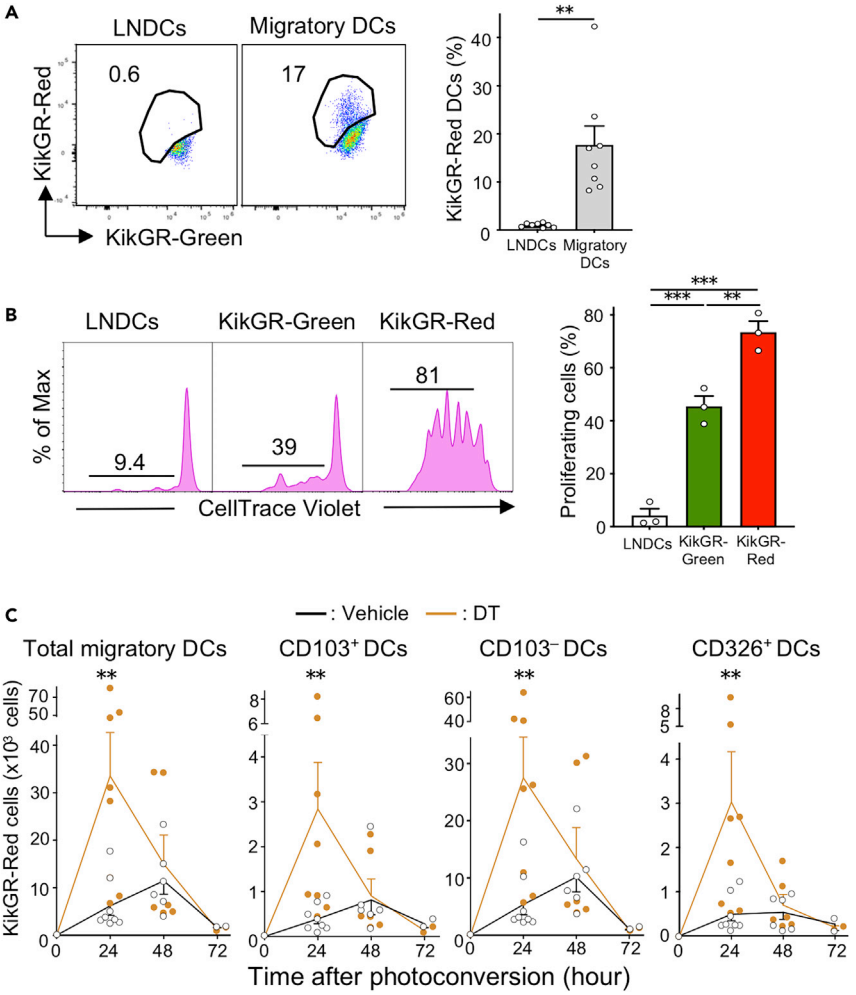

Figure 3. Tumor cell death enhances Ti-DC migration to dLNs

(A) Representative flow cytometry data of KikGR signals in CD11c^{high}MHC class II^{int} LNDCs and CD11c^{+}MHC class II^{high} migratory DCs in the dLN of KikGR mice 24 h after photoconversion (left). Proportions of KikGR-Red cells in each DC subset are shown (right). Bar graph shows means ± SEM of pooled data from four independent experiments (n = 8). **p < 0.01 (Mann-Whitney U test).

(B) Representative fluorescence intensity graph of CellTrace Violet in OT-I T cells co-cultured for 72 h with sorted DC subsets from dLNs of tumor-bearing KikGR mice 24 h after photoconversion. Numbers in histogram plots indicate proportion of proliferating cells identified by CellTrace Violet dilution (left). Bar graph shows summarized data of proportion of proliferating OT-I T cells (right). Bar graph shows means ± SEM of pooled data from two independent experiments (n = 3). **p < 0.01, ***p < 0.001 (one-way ANOVA with Holm-Sidak's multiple comparisons test).

(C) Number of KikGR-Red cells in MHC class II^{high} total migratory DCs and DC subsets in dLNs from vehicle or DT-treated tumor-bearing KikGR mice at indicated time points following photoconversion. Bar graph shows means ± SEM of pooled data from three (24, 48 h) or one (72 h) independent experiment (n = 2–8). **p < 0.01 (Mann-Whitney U test).

and DT treatment (Figure S5). These results suggest that ICD stimulates Ti-DC egress from tumors leading to rapid relocation of a large number of Ti-DCs to dLNs. Furthermore, this provides direct evidence of CD103^{+} Ti-DC migration from tumors to dLNs. This is particularly significant because this subset has been shown to play a dominant role in antigen trafficking to dLNs and subsequent presentation of tumor antigens to CD8^{+} T cells (Roberts et al., 2016).

Mechanism of immunogenic tumor cell death-induced DC migration

In ICD, ATP, HMGB1, and other DAMPs molecules released from dying cells stimulate the immune response (Krysko et al., 2012). ATP released from dying tumor cells interacts with Ti-DCs via one of the

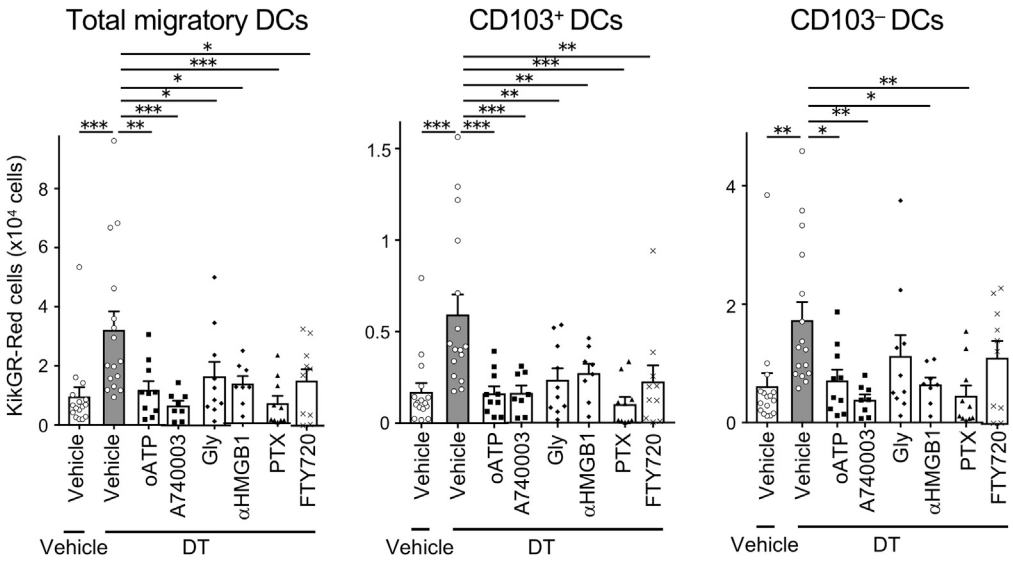

Figure 4. Tumor cell death enhanced CD103$^+$ Ti-DC migration to dLNs is inhibited by ATP-P2X7R, HMGB1-TLR4, Gαi-protein, and S1PR1 pathway blockade

Inhibitors were administrated together with DT at the time of tumor photoconversion and analyzed 24 h later. A number of KikGR-Red cells in total migratory DCs and DC subsets in dLNs. Bar graph shows means ± SEM of pooled data from at least two independent experiments (n = 8-16). *p < 0.05, **p < 0.01, ***p < 0.001 (one-way ANOVA with Holm-Sidak's multiple comparisons test).

ATP receptors, P2X7R, and enhances anti-tumor immunity (Ghiringhelli et al., 2009). HMGB1 activates immune cells by binding to TLR4 (Apetoh et al., 2007). We hypothesized that DAMPs may promote tumor immunity by enhancing Ti-DC migration to dLNs. Therefore, we used MC38/TfROVA-DTR to test this hypothesis by examining whether Ti-DC migration was modulated via HMGB1-TLR4 and/or ATP-P2X7R pathways. When tumors were photoconverted and ICD was induced, mice were simultaneously injected peritoneally with P2X7R antagonists, oxidized ATP (oATP) (Mutini et al., 1999; Zhao et al., 2016) or A-740003 (De Marchi et al., 2019). KikGR-Red migratory DCs were analyzed 24 h later (Figure S6). We found that injection of both antagonists counteracted ICD-induced increase in KikGR-Red total migratory, CD103$^+$ DCs, and CD103$^-$ DCs in dLNs, reducing migration to levels similar to steady-state migration. Glycyrrhizin (Gly), blocker of HMGB1 binding to TLR4 (Mollica et al., 2007; Yan et al., 2017), inhibited migration of KikGR-Red total migratory and CD103$^+$ Ti-DCs and tended to inhibit that of CD103 DCs. In addition, anti-HMGB1 antibody significantly inhibited migration of KikGR-Red total migratory, CD103$^+$, and CD103$^-$ Ti-DCs (Figure 4). These results suggested that enhanced CD103$^+$ and CD103$^-$ Ti-DC migration to dLNs elicited by ICD utilizes P2X7R and HMGB1 signaling pathways.

Steady-state Ti-DC migration is dependent on Gαi-protein-coupled chemokine receptor, CCR7, and thus can be blocked by an inhibitor of Gαi signaling, pertussis toxin (PTX) (Roberts et al., 2016). We examined whether enhanced Ti-DC migration after ICD induction is similarly suppressed by PTX treatment. PTX injection before tumor photoconversion and ICD induction significantly reduced KikGR-Red total migratory and CD103$^+$ and CD103$^-$ Ti-DC egress to dLNs, to a lower level than migration in the non-DT-treated group (Figure 4). This is probably due to the inhibitory effect of PTX on DC migration in steady state as well as on ICD-induced Ti-DC migration.

T cell migration from normal and inflamed peripheral tissues utilizes S1P-S1PR1 pathway (Ledgerwood et al., 2008; Nakanishi et al., 2017; Pappu et al., 2007; Tomura et al., 2010). However, the contribution of this pathway to DC egress from tissues is controversial (Lan et al., 2005). Furthermore, it is not known whether S1P-S1PR1 pathway contributes to Ti-DC egress after ICD induction. To test this, we administered FTY-720, which blocks the S1P-S1PR1 pathway. This treatment inhibited migration of total migratory DCs, CD103$^+$, and CD103$^-$ Ti-DCs to dLNs (Figure 4). These results suggested that enhanced migration of Ti-DCs after ICD induction is chemokine signaling dependent, and CD103$^+$ DCs use S1P1 pathway to egress tumors. Notably, CD103$^+$ DCs were more sensitive to FTY-720 inhibition than CD103$^-$ DCs, suggesting that CD103$^-$ DCs use additional signaling pathways to egress tumors.

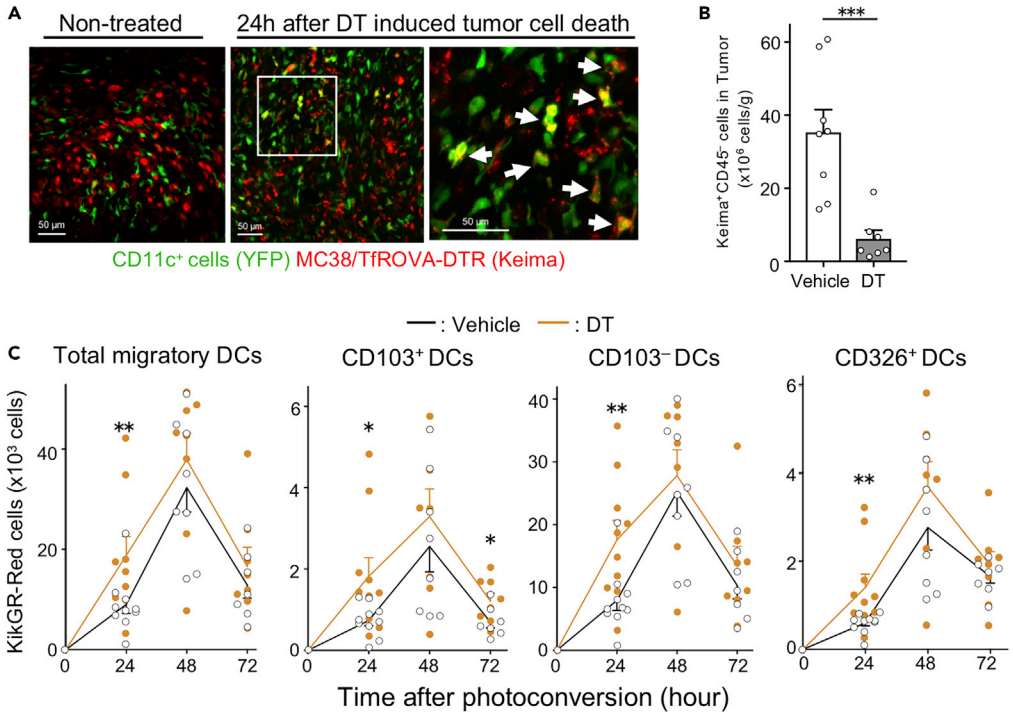

Figure 5. Partial tumor cell death induction accelerates Ti-DC migration

Tumors consisted of MC38/TfROVA-DTR and MC38 cells (mixed in the 3:7 ratio).

(A and B) Organs from CD11c-YFP mice bearing mixed tumors were analyzed 24 h after DT or vehicle treatment. Fluorescent microscopic images of tumors (A), number of Keima^{+}CD45^{-} cells (B). While arrows indicate YFP^{+} cells that phagocytosed dying tumor cells. Scale bar, 50 μm. Bar graph shows means ± SEM of pooled data from two independent experiments (n = 6–7). ***p < 0.001 (Mann-Whitney U test).

(C) Number of KikGR-Red cells in MHC class II^{high} total migratory DCs and DC subsets in dLNs from vehicle or DT-treated KikGR mice bearing mixed tumors at indicated time points following photoconversion. Bar graphs show means ± SEM of pooled data from two independent experiments (n = 7–10). *p < 0.05, **p < 0.01, ***p < 0.001. (Mann-Whitney U test).

Partial tumor cell death accelerates Ti-DC migration from tumors to dLNs

Our results indicate that inducing tumor cell death in a large proportion of tumor cells accelerates Ti-DC turnover within tumors and migration to dLNs. However, anti-tumor treatments, such as chemotherapy, do not typically kill all tumor cells. Thus, we next elucidated the effect of ICD on anti-tumor responses in a situation where most of the tumor cells survive and tumor mass remains. To do this we examined whether a lower proportion of killed tumor cells could also enhance myeloid cell phagocytosis and Ti-DC migration to dLNs. A mixture of MC38/TfROVA-DTR and MC38 cells (mixed in the 3:7 ratio) was inoculated in CD11c-YFP mice as in Figure 1B. Similarly to our earlier findings, YFP^{+} cells infiltrated tumors, but almost no YFP^{+} cells phagocytosed Keima-labeled tumor cells. However, after partial ICD was induced, YFP^{+} cells phagocytosed dying tumor cells (Figure 5A). DT administration in this system led to death of more than 85% of Keima^{+} MC38/TfROVA-DTR tumor cells (Figure 5B).

To analyze Ti-DC dynamics in tumors, KikGR mice were inoculated with a mixture of MC38/TfROVA-DTR and MC38 cells (3:7 ratio), and tumors were photoconverted as in Figure 2A. Time course study revealed that ICD induction modestly, but significantly, enhanced migration of total migratory DC and all Ti-DC subsets to the dLN (Figure 5C).

Immunogenic tumor cell death enhances tumor antigen-specific T cell proliferation

TLR ligands have been utilized as adjuvants to enhance immune responses. TLR4 ligand, LPS, induces DC maturation (Castiello et al., 2011). Furthermore, LPS analogs have been developed for use as adjuvants to enhance anti-tumor immune responses (Shetab Boushehri et al., 2018). As shown earlier, endogenous TLR4 ligand, HMGB-1 released from dying tumor cells induced Ti-DC migration. Although, LPS is not released by

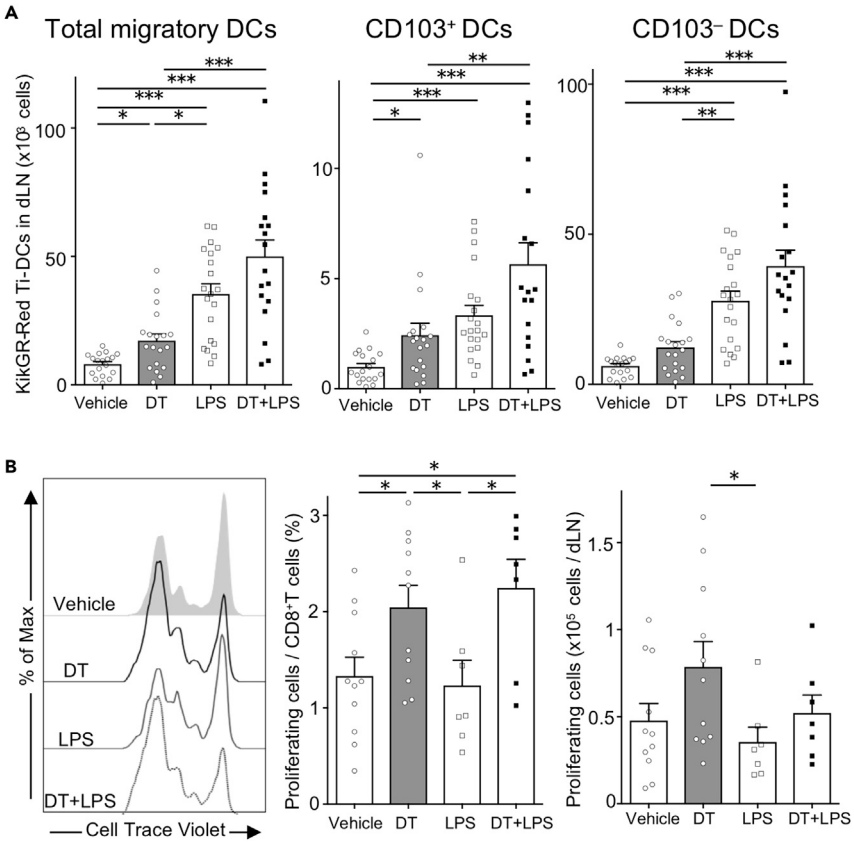

Figure 6. Ti-DC migration and antigen-specific CD8⁺ T cell proliferation after tumor cell death induction and LPS treatment

DT (intraperitoneal) and/or LPS (intratumoral) were administered to KikGR mice bearing mixed MC38/TfROVA-DTR and MC38 tumors (3:7 ratio) at time of photoconversion.

(A) Number of KikGR-Red cells in DCs in the dLNs from vehicle, DT-, and/or LPS-treated KikGR mice 24 h after tumor photoconversion. Bar graphs show means ± SEM of pooled data from at least nine independent experiments (n = 18–20). *p < 0.05, **p < 0.01, ***p < 0.001. (Kruskal-Wallis test with Dunn's comparisons test).

(B) Representative fluorescent intensity graph of CellTrace Violet of OT-I T cells, the proportion of proliferating OT-I T cells among CD8⁺ T cells, and the cell number of proliferating OT-I T cells in the dLNs 45 h after transfer to tumor bearing mice 24 h after vehicle, DT, and/or LPS treatment. Bar graphs show means ± SEM of pooled data from at least four independent experiments (n = 7–11). *p < 0.05. (Kruskal-Wallis test with Dunn's comparisons test).

dying tumor cells, it is important to study how this adjuvant affects DC migration and function in relation to ICD, because multiple studies have reported conflicting roles of LPS in modulating DC function (Klaska et al., 2017; Shen et al., 2008). To address these issues, we first examined the effect on Ti-DC migration in our system. Tumors grown from MC38/TfROVA-DTR and MC38 cells (mixed in the 3:7 ratio) in KikGR mice were photoconverted and LPS was injected directly into these tumors. Twenty-four hours later, we observed that the number of KikGR-Red total migratory Ti-DCs and CD103⁻ Ti-DCs in dLNs was increased to a much greater extent by LPS treatment than by ICD induction. Furthermore, DC migration was further enhanced by combining LPS treatment with ICD induction (Figure 6A).

We also observed that expression of costimulatory molecules CD80 and CD86 was the lowest in CD8α⁺ LNDCs and highest in KikGR-Red migratory CD103⁺ and CD103⁻ Ti-DCs regardless of treatment. In addition, CD86 expression in KikGR-Red cells was further upregulated after LPS injection compared with ICD induction alone. In contrast, whereas MHC class I expression was lower in CD8α⁺ LNDCs and higher in CD103⁺ and CD103⁻ DCs, its levels were not altered after LPS injection (Figure S7).

We next examined whether enhanced Ti-DC migration together with increased MHC class I and co-stimulatory molecule expression on Ti-DCs led to augmented proliferation of tumor-specific T cells *in vivo*. CellTrace

Violet-labeled OVA-specific OT-I T cells were adoptively transferred into MC38/TfROVA-DTRs and MC38 tumor-bearing mice and analyzed two days later. We observed that ICD induction, but not LPS, increased $CD8^+$ T cell proliferation (Figure 6B). Furthermore, combining LPS with ICD tended to reduce the number of proliferating tumor-specific $CD8^+$ T cells compared with ICD induction alone. These results suggest that ICD can enhance anti-tumor $CD8^+$ T cell proliferation *in vivo*. However, LPS-induced maturation and migration of Ti-DCs did not boost this further but may have inhibited anti-tumor T cell responses induced by ICD.

Immunogenic tumor cell death promotes antigen-specific $CD8^+$ effector T cell responses in dLNs and at distal tumor sites

Increased tumor-antigen-specific T cell proliferation after ICD induction in dLNs prompted us to investigate the effect of ICD on distal tumors and systemic immunity. At first, we analyzed endogenous tumor-antigen-specific T cells following ICD. Wild-type mice were inoculated with two tumors: MC38/TfROVA-DTR and MC38 cells (injected in the 3:7 ratio), and a distal secondary tumor, B16 melanoma cells expressing the same antigen (ovalbumin, B16-OVA). Five days later ICD was induced in the MC38 tumor (Figure 7A) and OVA-specific endogenous T cells were detected with H-$2K^b$ OVA tetramer-SIINFEKL. ICD induction led to a greater number of OVA-specific T cells in B16-OVA tumors and draining axillary LNs 2 and 10 days after ICD induction compared with untreated animals (Figure 7B). Next, we elucidated the effect of ICD on $CD8^+$ T cell effector/memory subsets 2 days after ICD induction (Figures 7C and S8). We observed that more MPECs were present in B16-OVA tumors after ICD induction, whereas DPECs and MPECs were significantly elevated in B16-OVA dLNs. These results indicate that inducing ICD can promote anti-tumor T cell responses.

Inducing immunogenic tumor cell death in primary tumors leads to the suppression of secondary tumor growth in a $CD103^+$ DC-dependent manner

We hypothesized that the increase in tumor antigen-specific T cells in secondary tumors following primary tumor cell death induction may affect secondary tumor growth. Thus, we evaluated anti-tumor immunity after ICD induction, LPS injection, and combination of both treatments by quantitating growth of secondary B16-OVA tumors. Mice were injected with a mixture of MC38/TfROVA-DTR and MC38 cells (3:7 ratio) and B16-OVA cells (as in Figure 7A) and 5 days later treated with DT, LPS, or DT and LPS as previously. We observed that partial ICD significantly suppressed B16-OVA growth, whereas treatment with LPS alone or in combination with ICD had only a slight effect on tumor growth (Figure 8A). The observed effect was not due to the direct suppression of B16-OVA growth by DT because B16-OVA growth was not altered in mice without MC38/TfROVA-DTRs regardless of DT treatment (Figure 8B). It was also not due to an abscopal effect because growth of B16 tumors not expressing OVA was not altered with or without partial cell death of MC38/TfROVA-DTRs (Figure 8C). These results suggested that consistent with increased tumor antigen-specific T cell proliferation (Figure 6B), inducing ICD leads to enhanced anti-tumor immunity. In contrast to ICD induction alone, LPS-induced Ti-DC maturation was less effective in controlling tumor growth. Furthermore, addition of LPS reduced the effect of ICD.

As Ti-DC emigration to dLNs was Gαi dependent (Figure 4), we examined whether inhibiting this migration will abrogate increased anti-tumor responses following ICD induction. To test this, we injected PTX at the same time as ICD was induced with DT (DT + PTX). Tumors grew significantly faster in mice treated with PTX even when ICD was induced with DT compared with mice that were treated with DT alone (Figure 8D). These results suggested that Ti-DC migration to dLNs is important for enhancing tumor immunity following ICD.

However, as PTX blocks migration of other immune cells as well as DCs, we looked for a specific contribution of $CD103^+$ DCs at the time of ICD to improve anti-tumor immune response following tumor cell death induction. We generated XCR1-$DTR^{+/-}$ mice, where $XCR1^+$ cells express DTR, and thus a single DT injection transiently depletes $CD103^+$ migratory DCs and $CD8\alpha^+$ LNDCs (Yamazaki et al., 2013). By concurrent ICD induction and transient removal of $CD103^+$ DCs, we investigated the importance of $CD103^+$ DCs during ICD induction. XCR1-$DTR^{+/-}$ or XCR1-$DTR^{-/-}$ wild type mice were inoculated with a mixture of MC38/TfROVA-DTRs and MC38 cells and B16-OVA as previously. Five days later tumor-bearing mice were treated with DT or vehicle. Compared with XCR1-$DTR^{+/-}$ control mice that received vehicle treatment (ICD(−),$CD103^+$ DC non-depleted), growth of B16-OVA tumors was strongly inhibited in XCR1-$DTR^{-/-}$ mice treated with DT (ICD(+), $CD103^+$DC non-depleted). However, transient depletion of $CD103^+$ DCs in XCR1-$DTR^{+/-}$ mice following DT administration (ICD(+), $CD103^+$ DC depleted) attenuated the tumor growth inhibitory effect of ICD to a level close to that of XCR1-$DTR^{+/-}$ vehicle treatment control mice

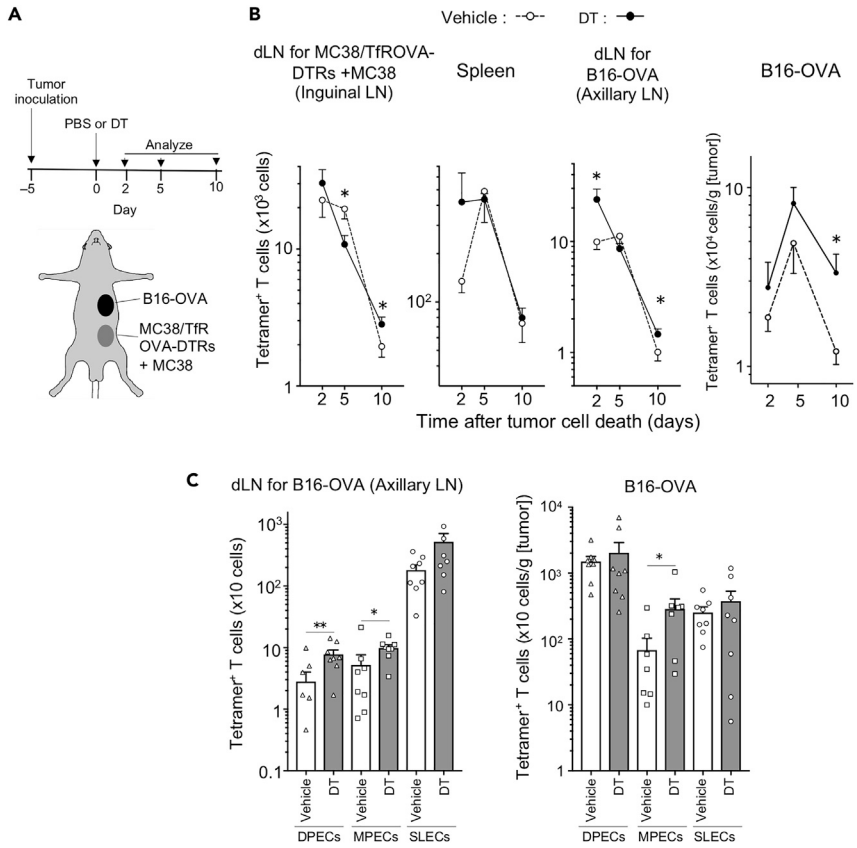

Figure 7. Partial tumor cell death induction increases tumor antigen-specific effector T cells

(A) Experimental setup for the analysis of endogenous tumor-antigen specific T cells after partial tumor cell death induction. Mixture of MC38/TfROVA-DTR and MC38 cells (3:7 ratio) was intradermally inoculated into abdominal skin, and B16-OVA tumor cells were subcutaneously inoculated into flank skin of C57BL/6 mice 5 days before tumor cell death induction. Tumor cell death was induced at day 0. Two, five, and ten days later, endogenous tumor-antigen-specific T cells were analyzed.

(B) Number of OVA tetramer$^+$ CD8$^+$ T cells at indicated time points following DT or vehicle treatment. Line graphs show means ± SEM of pooled data from at least two independent experiments (n = 8–12). *p < 0.05 (Mann-Whitney U test).

(C) Number of DPEC, MPEC, and SLEC in OVA tetramer$^+$ CD8$^+$ T cells 2 days following vehicle or DT treatment. Bar graphs show means ± SEM of pooled data from two independent experiments (n = 8). As values of two samples of DEPCs in axillary LN from Vehicle group and 1 sample of MEPCs in Tumor from Vehicle and DT groups were zero, these data were not shown in these figures. *p < 0.05, **p < 0.01 (Mann-Whitney U test).

(Figure 8E). These results suggested that CD103$^+$ DCs are necessary at the time of ICD induction to improve systemic anti-tumor immune responses following ICD.

DISCUSSION

In this study, by combining *in vivo* ICD induction via DT treatment with intravital photolabeling in KikGR mice, we have established a system that allowed us to exclude the confounding effects of chemo- and radiotherapy and quantify cell migration during ICD induction. Taking advantage of this system, we examined kinetics of Ti-DC and other myeloid cell turnover in tumors, characterized retention and egress of different subsets in response to ICD, and showed that DCs were more sensitive to ICD enhancement compared with other myeloid cells. Furthermore, we show that inducing ICD *in situ* accelerated CD103$^+$ Ti-DC phagocytosis, turnover within tumors, and emigration to dLNs. This led to increased tumor antigen-specific CD8$^+$ T cells and suppression of secondary tumor growth. DAMPs molecules released by dying tumor cells, including ATP and HMGB1, accelerated CD103$^+$ and CD103$^-$ Ti-DC migration from tumors to dLNs via P2X7R and TLR4 signaling pathways. However, combining tumor cell death induction with LPS treatment stimulated Ti-DC maturation and emigration to dLNs but reduced the effect of tumor cell

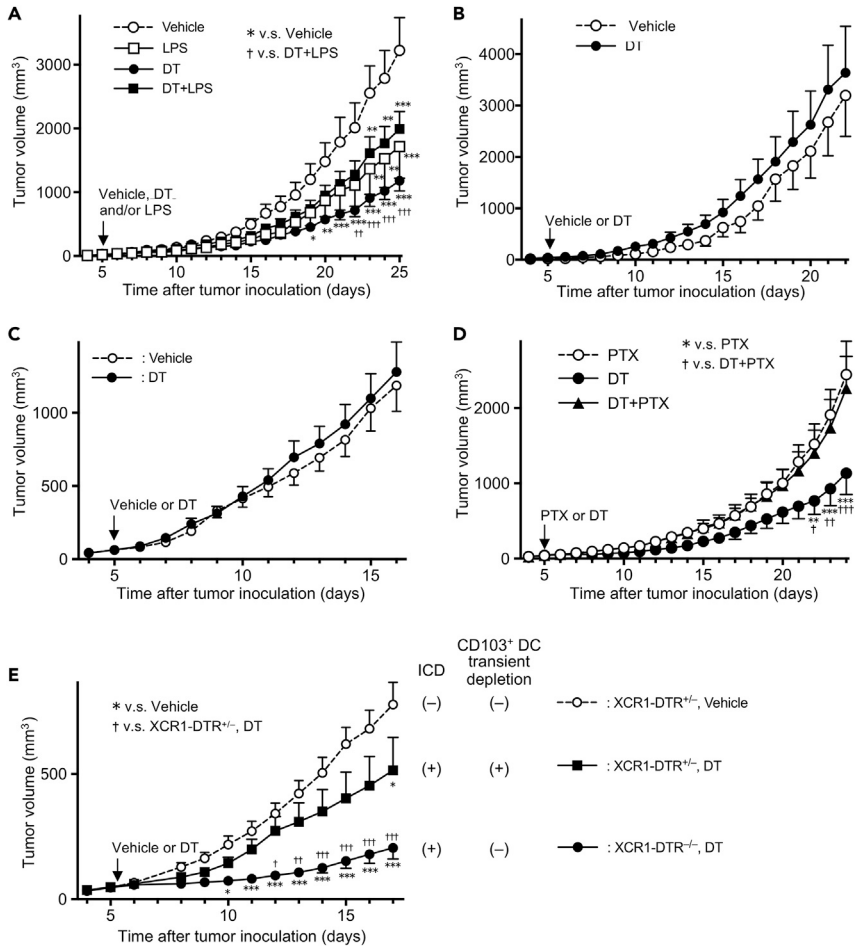

Figure 8. Tumor cell death induction suppresses secondary tumor growth in CD103$^+$ DCs and cell migration-dependent manner

(A, D, and E) A mixture of MC38/TfROVA-DTR and MC38 cells (3:7 ratio) and B16-OVA tumor cells were intradermally and subcutaneously inoculated into abdominal and flank skin of C57BL/6 mice (A and D), or XCR1-DTR$^{+/-}$ or XCR1-DTR$^{-/-}$ wild type littermate mice (E), respectively.

(B) MC38 and B16-OVA tumor cells were intradermally and subcutaneously inoculated into abdominal and flank skin of C57BL/6 mice, respectively.

(C) A mixture of MC38/TfROVA-DTR and MC38 cells (3:7 ratio) and B16 tumor cells were intradermally and subcutaneously inoculated into abdominal and flank skin of C57BL/6 mice, respectively. Five days following tumor inoculation, tumor-bearing mice were treated with vehicle, LPS, DT, and LPS + DT (A), vehicle and DT (B, C, and E), PTX, DT, and PTX + DT (D). Line graphs show means ± SEM of pooled data of B16-OVA (A, B, D, E) or B16 (C) volumes obtained in a representative experiment (A: n = 6–8, B: n = 5 or 6, C: n = 12, D: n = 8–10, E: n = 6–12). All experiments were performed at least two times. v.s. Vehicle (A, E) or PTX (D) *$p < 0.05$, **$p < 0.01$, ***$p < 0.001$; v.s. DT + LPS (A), DT + PTX (D), or DT-treated XCR1-DTR$^{+/-}$ (E); $^{\dagger}p < 0.05$, $^{\dagger\dagger}p < 0.01$, $^{\dagger\dagger\dagger}p < 0.001$ (two-way ANOVA with Sidak's multiple comparisons test).

death-induced tumor growth suppression. Finally, we demonstrate that immune cell migration at the time of ICD induction is crucial for tumor cell death-induced suppression of tumor growth. Furthermore, our results add to a substantial body of literature on ICD in tumors and suggest that our findings about the effect of ICD on myeloid cell turnover, migration, and function are useful in understanding tumor immunity where ICD is induced by chemo- or radiotherapy.

Using tumor-bearing KikGR mice, we showed that only a small proportion of MoDCs remains in the tumors after 24 h, regardless of ICD induction. This indicated that the majority of MoDCs in tumors turnover within 24 h and the effect of ICD on MoDC dynamics is limited. Future studies will identify the exact fate of Ti-MoDCs: whether they die *in situ* and/or migrate to dLNs. In contrast to MoDCs, ICD reduced the number

of KikGR-Red CD103$^+$ and CD103$^-$ Ti-DCs remaining in tumors after 24 h. Concomitant with this, the number of KikGR-Red DCs in dLNs peaked early and started to decline by 48 h following tumor photoconversion and ICD induction. Notably, KikGR-Red Ti-DCs did not accumulate in dLNs. We previously reported that the lifetime of skin migratory DC subsets in dLNs is less than 1 day in the tape-stripping model of inflammation and skin migratory DCs do not egress the dLN (Tomura et al., 2014). It is plausible that the lifetime of Ti-DCs is similarly short in the inflammatory milieu of the tumor microenvironment and Ti-DCs that migrated to the dLN would then die *in situ* without egressing the dLN.

In addition, we analyzed phenotypes of Ti-DCs in dLN by comparing KikGR-Red migratory DCs that emigrated from tumors to KikGR-Green migratory DCs that either migrated from tumors before photoconversion or came to dLNs from other sites. Tumor-derived migratory DCs in dLNs expressed higher level of co-stimulatory molecules and had a higher capacity to induce proliferation of naive antigen-specific CD8$^+$ T cells compared with that of KikGR-Green migratory DCs. These results suggest that the tumor microenvironment, which includes inflammatory cytokines in the tumor parenchyma, may stimulate DC function.

We observed that a small number of CD103$^+$ DCs were localized at the edge of solid tumors and almost no CD103$^+$ DCs were observed within the tumor mass. This result is in line with an earlier report that CD103$^+$ DCs are sparse in proximity to tumor margins but plentiful in distal regions in PYMT mice (Broz et al., 2014). However, after inducing ICD, CD103$^+$ DCs accumulated inside the tumor and phagocytosed dying tumor cells. ATP accelerates DC migration (Sáez et al., 2017), whereas DAMPs signals promote opsonization or phagocytosis of dying cancer cells (Gardai et al., 2005; Garg et al., 2012a, 2012b). Thus, it is plausible that DAMPs molecules released from dying tumor cells induce DC accumulation within tumor and promote phagocytosis by CD103$^+$ DCs.

PTX strongly inhibited CD103$^+$ DC migration to dLNs. In contrast, blocking ATP-P2X7R or HMGB1-TLR4 pathways abrogated ICD induced increase in CD103$^+$ DC migration but only to basal level (without induced tumor cell death). These results suggest that the molecular mechanisms of spontaneous Ti-DC migration are regulated through pathways additional to ATP-P2X7R or HMGB1-TLR4.

TLR4 ligand, LPS, stimulated DC maturation and migration as well as CD86 upregulation, but did not promote generation of antigen-specific CD8$^+$ T cells in dLNs. It is possible that in the case of simultaneous ICD induction and LPS injection, Ti-DCs lose phagocytic activity due to maturation (Wilson et al., 2006) even in the presence of dying tumor cells. In addition to DC maturation, LPS induces DC apoptosis by NAFT activation through CD14 (Zanoni et al., 2009), suggesting that the strong stimulation of TLR4 by LPS accelerated Ti-DC death and shortened the antigen presentation period of DCs. These could lead to a lower efficiency of antigen presentation and antigen-specific T cell stimulation in dLNs and attenuation of ICD-induced tumor regression. Alternatively, LPS may counteract the anti-tumor effect of ICD by inducing IL-10 and DC tolerance (endotoxin-tolerized DCs) (Klaska et al., 2017). LPS can induce IL-10-secreting DCs that promote generation of CD62L-expressing Tregs and suppress experimental autoimmune uveoretinitis (Lau et al., 2008).

Inducing ICD *in situ* led to an increase in antigen-specific CD8$^+$ T cells in secondary tumors. Specifically, we observed increased numbers of MPECs and DEPCs. MPECs contribute to long-term anti-tumor responses (Kobayashi et al., 2015). They phenotypically resemble SLECs and produce comparable level of IFN-γ (Kobayashi et al., 2015). In addition, it has been proposed that DPECs may represent a long-lived effector cell population with capacity for proliferation and potential to become memory cells (Steffensen et al., 2013). In fact, DEPCs were the major population in B16-OVA tumors in our model, and it is possible that the anti-tumor effect of ICD is mediated through enhanced MPEC and DPEC response. Increased number of these cells may lead to effective long-term anti-tumor immunity.

Indirect presentation pathways, where CD103$^-$ DCs carry the antigen to dLNs, play a role in priming CD8$^+$ T cells. It has been reported that CD103$^-$ DCs (cDC2) have the highest Th17-inducing ability (Laoui et al., 2016) among DC subsets, and thus it is possible that CD103$^-$ DCs enhance anti-tumor immune response via Th17 generation. Th17 cells have also been reported to acquire MHC class I$^+$ tumor antigen-derived peptides by trogocytosis and stimulating antigen-specific CD8$^+$ T cells (Ankathatti Munegowda et al., 2011). Although the role of MoDCs in the ICD-induced suppression of distal tumor growth is unclear, an earlier study suggested that MoDCs rather than CD103$^+$ DCs are responsible for the ICD-induced anti-cancer effects in the primary tumor (Ma et al., 2013). Thus, it is possible that enhanced CD103$^-$ DC migration to dLNs

induced by ICD and MoDCs in primary tumors together contribute to increased systemic anti-tumor immunity. However, we think that, at least in our system, the contribution of non-CD103$^+$ DC subsets, such as CD103$^-$ DCs and MoDCs, to systemic anti-tumor immune responses following ICD induction is limited. On the other hand, the requirement for CD103$^+$ DCs at the time of ICD induction, coupled with a report that tumor growth suppression elicited by killed tumor cell immunization is completely abrogated in BATF3$^{-/-}$ mice, which lack CD103$^+$ DCs (Jaime-Sanchez et al., 2020), suggests that CD103$^+$ DCs are the main subset responsible for inhibition of secondary tumor growth. Although a specific tumor system was used in our study to demonstrate the effect of ICD on turnover and migration of antigen-presenting cells in cancer, our findings that CD103$^+$ DCs migrating from the tumor to the dLN are important for enhancing the systemic anti-tumor immune response induced by ICD are applicable to other tumor settings where ICD is induced *in situ* by chemotherapy or radiotherapy.

We have demonstrated the effect of ICD on anti-tumor immune responses by eliminating the immunosuppressive effects of chemotherapy and irradiation. In clinic, attempts have been made to use dying immunogenic cells induced by chemotherapy or irradiation therapy to enhance anti-tumor immunity (Wang et al., 2018). However, rapid Ti-DC turnover in our tumor model suggests that continuous supply of DC precursors from the bone marrow is crucial for induction and maintenance of Ti-DCs involved in stimulating anti-tumor antigen-specific CD8$^+$ T cell response. The supply of Ti-DC precursor cells may be affected by bone marrow suppression. Thus, anti-tumor therapy should aim to minimize bone marrow suppression to achieve enhancement of the anti-tumor response by ICD.

Limitations of the study

A potential caveat of this work is that the effects of ICD on anti-tumor responses with or without LPS treatment have been examined *in vivo* in one tumor model only.

Resource availability

Lead contact

Requests for further information and and reagents should be directed to and will be fulfilled by the lead contact, Michio Tomura (michio.tomura@gmail.com).

Materials availability

Materials generated in this study are available upon request.

Data and code availability

This study did not generate/analyze datasets or code.

METHODS

All methods can be found in the accompanying Transparent methods supplemental file.

SUPPLEMENTAL INFORMATION

Supplemental information can be found online at https://doi.org/10.1016/j.isci.2021.102424.

ACKNOWLEDGMENTS

This work was supported in part by JSPS Grants-in-Aid for Scientific Research in Innovative Areas ''Analysis and Synthesis of Multidimensional Immune Organ Network'' (#24111007); JSPS Grants-in-Aid for Scientific Research (B) (#16H05087); Special Coordination Funds for Promoting Science and Technology of the Japanese Government; National Health and Medical Research Council Australia project grants GNT1106043 (T.C.), National Breast Cancer Foundation grant IIRS-19-027 (T.C.), Pankind Foundation grant (T.C.), Perpetual Impact grant (T.C.), and Astellas Pharma Inc. through the Formation of Innovation Centers for the Fusion of Advanced Technologies Program.

AUTHOR CONTRIBUTIONS

T.M., S.U., R.I, I.Y., Y.N., K.M., Y.K, T.C., and M.T. designed experiments. T.M., K.Kitagawa, Y.H., and M.U. performed experiments. H.H. and T.K. prepared XCR1-Venus mice and XCR1-DTR mice. T.H. and K.Kabashima prepared CD11c-YFP mice. T.M. and M.T. analyzed data. T.M., T.C., and M.T. wrote the manuscript.

DECLARATION OF INTERESTS

The authors declare no competing interests.

Received: April 29, 2020
Revised: February 4, 2021
Accepted: April 9, 2021
Published: May 21, 2021

REFERENCES

Abbas, A., Lichtman, A., and Pillai, S. (2015). Cellular and Molecular Immunology, International Edition, 8th (Philadelphia: Elsevier Saunders).

Ankathatti Munegowda, M., Deng, Y., Mulligan, S.J., and Xiang, J. (2011). Th17 and Th17-stimulated CD8+ T cells play a distinct role in Th17-induced preventive and therapeutic antitumor immunity. Cancer Immunol. Immunother. *60*, 1473–1484. https://doi.org/10.1007/s00262-011-1054-y.

Apetoh, L., Ghiringhelli, F., Tesniere, A., Obeid, M., Ortiz, C., Criollo, A., Mignot, G., Maiuri, M.C., Ullrich, E., Saulnier, P., et al. (2007). Toll-like receptor 4-dependent contribution of the immune system to anticancer chemotherapy and radiotherapy. Nat. Med. *13*, 1050–1059. https://doi.org/10.1038/nm1622.

Asano, K., Nabeyama, A., Miyake, Y., Qiu, C.-H., Kurita, A., Tomura, M., Kanagawa, O., Fujii, S., and Tanaka, M. (2011). CD169-positive macrophages dominate antitumor immunity by crosspresenting dead cell-associated antigens. Immunity *34*, 85–95. https://doi.org/10.1016/j.immuni.2010.12.011.

Böttcher, J.P., and Reis e Sousa, C. (2018). The role of type 1 conventional dendritic cells in cancer immunity. Trends Cancer. https://doi.org/10.1016/j.trecan.2018.09.001.

Broz, M.L., Binnewies, M., Boldajipour, B., Nelson, A.E., Pollack, J.L., Erle, D.J., Barczak, A., Rosenblum, M.D., Daud, A., Barber, D.L., et al. (2014). Article dissecting the tumor myeloid compartment reveals rare activating antigen-presenting cells critical for T cell immunity. Cancer Cell *26*, 638–652. https://doi.org/10.1016/j.ccell.2014.09.007.

Casares, N., Pequignot, M.O., Tesniere, A., Ghiringhelli, F., Roux, S., Chaput, N., Schmitt, E., Hamai, A., Hervas-Stubbs, S., Obeid, M., et al. (2005). Caspase-dependent immunogenicity of doxorubicin-induced tumor cell death. J. Exp. Med. *202*, 1691–1701. https://doi.org/10.1084/jem.20050915.

Castiello, L., Sabatino, M., Jin, P., Clayberger, C., Marincola, F.M., Krensky, A.M., and Stroncek, D.F. (2011). Monocyte-derived DC maturation strategies and related pathways: a transcriptional view. Cancer Immunol. Immunother. *60*, 457–466. https://doi.org/10.1007/s00262-010-0954-6.

De Marchi, E., Orioli, E., Pegoraro, A., Sangaletti, S., Portararo, P., Curti, A., Colombo, M.P., Di Virgilio, F., and Adinolfi, E. (2019). The P2X7 receptor modulates immune cells infiltration, ectonucleotidases expression and extracellular ATP levels in the tumor microenvironment. Oncogene *38*, 3636–3650. https://doi.org/10.1038/s41388-019-0684-y.

Durgeau, A., Virk, Y., Corgnac, S., and Mami-Chouaib, F. (2018). Recent advances in targeting CD8 T-cell immunity for more effective cancer immunotherapy. Front. Immunol. *9*, 14. https://doi.org/10.3389/fimmu.2018.00014.

Fucikova, J., Kralikova, P., Fialova, A., Brtnicky, T., Rob, L., Bartunkova, J., and Špíšek, R. (2011). Human tumor cells killed by anthracyclines induce a tumor-specific immune response. Cancer Res. *71*, 4821–4833. https://doi.org/10.1158/0008-5472.CAN-11-0950.

Galluzzi, L., Buqué, A., Kepp, O., Zitvogel, L., and Kroemer, G. (2017). Immunogenic cell death in cancer and infectious disease. Nat. Rev. Immunol. *17*, 97–111. https://doi.org/10.1038/nri.2016.107.

Gardai, S.J., McPhillips, K.A., Frasch, S.C., Janssen, W.J., Starefeldt, A., Murphy-Ullrich, J.E., Bratton, D.L., Oldenborg, P.A., Michalak, M., and Henson, P.M. (2005). Cell-surface calreticulin initiates clearance of viable or apoptotic cells through trans-activation of LRP on the phagocyte. Cell. https://doi.org/10.1016/j.cell.2005.08.032.

Garg, A.D., Krysko, D.V., Vandenabeele, P., and Agostinis, P. (2012a). Hypericin-based photodynamic therapy induces surface exposure of damage-associated molecular patterns like HSP70 and calreticulin. Cancer Immunol. Immunother. *61*, 215–221. https://doi.org/10.1007/s00262-011-1184-2.

Garg, A.D., Krysko, D.V., Verfaillie, T., Kaczmarek, A., Ferreira, G.B., Marysael, T., Rubio, N., Firczuk, M., Mathieu, C., Roebroek, A.J.M., et al. (2012b). A novel pathway combining calreticulin exposure and ATP secretion in immunogenic cancer cell death. EMBO J. *31*, 1062–1079. https://doi.org/10.1038/emboj.2011.497.

Ghiringhelli, F., Apetoh, L., Tesniere, A., Aymeric, L., Ma, Y., Ortiz, C., Vermaelen, K., Panaretakis, T., Mignot, G., Ullrich, E., et al. (2009). Activation of the NLRP3 inflammasome in dendritic cells induces IL-1B-dependent adaptive immunity against tumors. Nat. Med. *15*, 1170–1178. https://doi.org/10.1038/nm.2028.

Hato, S.V., Khong, A., De Vries, I.J.M., and Lesterhuis, W.J. (2014). Molecular Pathways : the immunogenic effects of platinum- based chemotherapeutics. Clin. Cancer Res. https://doi.org/10.1158/1078-0432.CCR-13-3141.

Henri, S., Poulin, L.F., Tamoutounour, S., Ardouin, L., Guilliams, M., De Bovis, B., Devilard, E., Viret, C., Azukizawa, H., Kissenpfennig, A., and Malissen, B. (2010). CD207+ CD103+ dermal dendritic cells cross-present keratinocyte-derived antigens irrespective of the presence of Langerhans cells. J. Exp. Med. *207*, 189–206. https://doi.org/10.1084/jem.20091964.

Jaime-Sanchez, P., Uranga-Murillo, I., Aguilo, N., Khouili, S.C., Arias, M.A., Sancho, D., and Pardo, J. (2020). Cell death induced by cytotoxic CD8 + T cells is immunogenic and primes caspase-3-dependent spread immunity against endogenous tumor antigens. J. Immunother. Cancer *8*, https://doi.org/10.1136/jitc-2020-000528.

Joshi, N.S., Cui, W., Chandele, A., Lee, H.K., Urso, D.R., Hagman, J., Gapin, L., and Kaech, S.M. (2007). Inflammation directs memory precursor and short-lived effector CD8(+) T cell fates via the graded expression of T-bet transcription factor. Immunity *27*, 281–295. https://doi.org/10.1016/j.immuni.2007.07.010.

Klaska, I.P., Muckersie, E., Martin-Granados, C., Christofi, M., and Forrester, J.V. (2017). Lipopolysaccharide-primed heterotolerant dendritic cells suppress experimental autoimmune uveoretinitis by multiple mechanisms. Immunology *150*, 364–377. https://doi.org/10.1111/imm.12691.

Kobayashi, T., Doff, B.L., Rearden, R.C., Leggatt, G.R., and Mattarollo, S.R. (2015). NKT cell-targeted vaccination plus anti-4-1BB antibody generates persistent CD8 T cell immunity against B cell lymphoma. Oncoimmunology *4*, e990793. https://doi.org/10.4161/2162402X.2014.990793.

Kogure, T., Karasawa, S., Araki, T., Saito, K., Kinjo, M., and Miyawaki, A. (2006). A fluorescent variant of a protein from the stony coral Montipora facilitates dual-color single-laser fluorescence cross-correlation spectroscopy. Nat. Biotechnol. *24*, 577–581. https://doi.org/10.1038/nbt1207.

Krysko, D.V., Garg, A.D., Kaczmarek, A., Krysko, O., Agostinis, P., and Vandenabeele, P. (2012). Immunogenic cell death and DAMPs in cancer therapy. Nat. Rev. Cancer *12*, 860–875. https://doi.org/10.1038/nrc3380.

Lan, Y.Y., De Creus, A., Colvin, B.L., Abe, M., Brinkmann, V., Coates, P.T.H., and Thomson, A.W. (2005). The sphingosine-1-phosphate receptor agonist FTY720 modulates dendritic cell trafficking in vivo. Am. J. Transpl. *5*, 2649–2659. https://doi.org/10.1111/j.1600-6143.2005.01085.x.

Laoui, D., Keirsse, J., Morias, Y., Van Overmeire, E., Geeraerts, X., Elkrim, Y., Kiss, M., Bolli, E., Lahmar, Q., Sichien, D., et al. (2016). The tumour microenvironment harbours ontogenically distinct dendritic cell populations with opposing effects on tumour immunity. Nat. Commun. *7*, 1–17. https://doi.org/10.1038/ncomms13720.

Lau, A.W.T., Biester, S., Cornall, R.J., and Forrester, J.V. (2008). Lipopolysaccharide-activated IL-10-secreting dendritic cells suppress experimental autoimmune uveoretinitis by MHCII-dependent activation of CD62L-expressing regulatory T cells. J. Immunol. *180*, 3889–3899. https://doi.org/10.4049/JIMMUNOL.180.6.3889.

Ledgerwood, L.G., Lal, G., Zhang, N., Garin, A., Esses, S.J., Ginhoux, F., Merad, M., Peche, H., Lira, S.A., Ding, Y., et al. (2008). The sphingosine 1-phosphate receptor 1 causes tissue retention by inhibiting the entry of peripheral tissue T lymphocytes into afferent lymphatics. Nat. Immunol. *9*, 42–53. https://doi.org/10.1038/ni1534.

Lindquist, R.L., Shakhar, G., Dudziak, D., Wardemann, H., Eisenreich, T., Dustin, M.L., and Nussenzweig, M.C. (2004). Visualizing dendritic cell networks in vivo. Nat. Immunol. *5*, 1243–1250. https://doi.org/10.1038/ni1139.

Ma, Y., Adjemian, S., Mattarollo, S.R., Yamazaki, T., Aymeric, L., Yang, H., Portela Catani, J.P., Hannani, D., Duret, H., Steegh, K., et al. (2013). Anticancer chemotherapy-induced intratumoral recruitment and differentiation of antigen-presenting cells. Immunity *38*, 729–741. https://doi.org/10.1016/j.immuni.2013.03.003.

Mollica, L., De Marchis, F., Spitaleri, A., Dallacosta, C., Pennacchini, D., Zamai, M., Agresti, A., Trisciuoglio, L., Musco, G., and Bianchi, M.E. (2007). Glycyrrhizin binds to high-mobility group box 1 protein and inhibits its cytokine activities. Chem. Biol. *14*, 431–441. https://doi.org/10.1016/j.chembiol.2007.03.007.

Montico, B., Nigro, A., Casolaro, V., and Dal Col, J. (2018). Immunogenic apoptosis as a novel tool for anticancer vaccine development. Int. J. Mol. Sci. *19*, https://doi.org/10.3390/ijms19020594.

Mutini, C., Falzoni, S., Ferrari, D., Chiozzi, P., Morelli, A., Baricordi, O.R., Collo, G., Ricciardi-Castagnoli, P., and Di Virgilio, F. (1999). Mouse dendritic cells express the P2X7 purinergic receptor: characterization and possible participation in antigen presentation. J. Immunol. *163*, 1958–1965.

Nakanishi, Y., Ikebuchi, R., Chtanova, T., Kusumoto, Y., Okuyama, H., Moriya, T., Honda, T., Kabashima, K., Watanabe, T., Sakai, Y., and Tomura, M. (2017). Regulatory T cells with superior immunosuppressive capacity emigrate from the inflamed colon to draining lymph nodes. Mucosal Immunol *11*, 437–448. https://doi.org/10.1038/mi.2017.64.

Pappu, R., Schwab, S.R., Cornelissen, I., Pereira, J.P., Regard, J.B., Xu, Y., Camerer, E., Zheng, Y.W., Huang, Y., Cyster, J.G., and Coughlin, S.R. (2007). Promotion of lymphocyte egress into blood and lymph by distinct sources of sphingosine-1-phosphate. Science *316*, 295–298. https://doi.org/10.1126/science.1139221.

Pashenkov, M., Goëss, G., Wagner, C., Hörmann, M., Jandl, T., Moser, A., Britten, C.M., Smolle, J., Koller, S., Mauch, C., et al. (2006). Phase II trial of a toll-like receptor 9-activating oligonucleotide in patients with metastatic melanoma. J. Clin. Oncol. *24*, 5716–5724. https://doi.org/10.1200/JCO.2006.07.9129.

Roberts, E.W., Broz, M.L., Binnewies, M., Headley, M.B., Nelson, A.E., Wolf, D.M., Kaisho, T., Bogunovic, D., Bhardwaj, N., and Krummel, M.F. (2016). Critical role for CD103+/CD141+ dendritic cells bearing CCR7 for tumor antigen trafficking and priming of T cell immunity in melanoma. Cancer Cell *30*, 324–336. https://doi.org/10.1016/j.ccell.2016.06.003.

Sadozai, H., Gruber, T., Hunger, R.E., and Schenk, M. (2017). Recent successes and future directions in immunotherapy of cutaneous melanoma. Front. Immunol. *8*, 1617. https://doi.org/10.3389/fimmu.2017.01617.

Sáez, P.J., Vargas, P., Shoji, K.F., Harcha, P.A., Lennon-Duménil, A.-M., and Sáez, J.C. (2017). ATP promotes the fast migration of dendritic cells through the activity of pannexin 1 channels and $P2X_7$ receptors. Sci. Signal. *10*, eaah7107. https://doi.org/10.1126/scisignal.aah7107.

Saito, M., Iwawaki, T., Taya, C., Yonekawa, H., Noda, M., Inui, Y., Mekada, E., Kimata, Y., Tsuru, A., and Kohno, K. (2001). Diphtheria toxin receptor-mediated conditional and targeted cell ablation in transgenic mice. Nat. Biotechnol. *19*, 746–750. https://doi.org/10.1038/90795.

Salmon, H., Idoyaga, J., Rahman, A., Leboeuf, M., Remark, R., Jordan, S., Casanova-Acebes, M., Khudoynazarova, M., Agudo, J., Tung, N., et al. (2016). Expansion and activation of CD103+ dendritic cell progenitors at the tumor site enhances tumor responses to therapeutic PD-L1 and BRAF inhibition. Immunity *44*, 924–938. https://doi.org/10.1016/j.immuni.2016.03.012.

Shen, H., Tesar, B.M., Walker, W.E., and Goldstein, D.R. (2008). Dual signaling of MyD88 and TRIF is critical for maximal TLR4-induced dendritic cell maturation. J. Immunol. *181*, 1849–1858. https://doi.org/10.4049/jimmunol.181.3.1849.

Shetab Boushehri, M.A., Abdel-Mottaleb, M.M.A., Béduneau, A., Pellequer, Y., and Lamprecht, A. (2018). A nanoparticle-based approach to improve the outcome of cancer active immunotherapy with lipopolysaccharides. Drug Deliv. *25*, 1414–1425. https://doi.org/10.1080/10717544.2018.1469684.

Steffensen, M.A., Holst, P.J., Steengaard, S.S., Jensen, B.A.H., Bartholdy, C., Stryhn, A., Christensen, J.P., and Thomsen, A.R. (2013). Qualitative and quantitative analysis of adenovirus type 5 vector-induced memory CD8 T cells: not as bad as their reputation. J. Virol. *87*, 6283–6295. https://doi.org/10.1128/jvi.00465-13.

Teasdale, R.D., D'Agostaro, G., and Gleeson, P.A. (1992). The signal for golgi retention of bovine β1,4-galactosyltransferase is in the transmembrane domain. J. Biol. Chem. *267*, 4084–4096.

Tomura, M., Hata, A., Matsuoka, S., Shand, F.H.W., Nakanishi, Y., Ikebuchi, R., Ueha, S., Tsutsui, H., Inaba, K., Matsushima, K., et al. (2014). Tracking and quantification of dendritic cell migration and antigen trafficking between the skin and lymph nodes. Sci. Rep. *4*, 1–11. https://doi.org/10.1038/srep06030.

Tomura, M., Itoh, K., Kanagawa, O., and Alerts, E. (2010). Naive CD4+ T lymphocytes circulate through lymphoid organs to interact with endogenous antigens and upregulate their function. J. Immunol. *184*, 4646–4653. https://doi.org/10.4049/jimmunol.0903946.

Torcellan, T., Hampton, H.R., Bailey, J., Tomura, M., Brink, R., and Chtanova, T. (2017). In vivo photolabeling of tumor-infiltrating cells reveals highly regulated egress of T-cell subsets from tumors. Proc. Natl. Acad. Sci. U. S. A. https://doi.org/10.1073/pnas.1618446114.

Wang, Q., Ju, X., Wang, J., Fan, Y., Ren, M., and Zhang, H. (2018). Immunogenic cell death in anticancer chemotherapy and its impact on clinical studies. Cancer Lett. https://doi.org/10.1016/j.canlet.2018.08.028.

Wilson, N.S., Behrens, G.M.N., Lundie, R.J., Smith, C.M., Waithman, J., Young, L., Forehan, S.P., Mount, A., Steptoe, R.J., Shortman, K.D., et al. (2006). Systemic activation of dendritic cells by Toll-like receptor ligands or malaria infection impairs cross-presentation and antiviral immunity. Nat. Immunol. *7*, 165–172. https://doi.org/10.1038/ni1300.

Yamazaki, C., Sugiyama, M., Ohta, T., Hemmi, H., Hamada, E., Sasaki, I., Fukuda, Y., Yano, T., Nobuoka, M., Hirashima, T., et al. (2013). Critical roles of a dendritic cell subset expressing a chemokine receptor, XCR1. J. Immunol. *190*, 6071–6082. https://doi.org/10.4049/jimmunol.1202798.

Yan, B., Chen, F., Xu, L., Xing, J., and Wang, X. (2017). HMGB1-TLR4-IL23-IL17A axis promotes paraquat-induced acute lung injury by mediating neutrophil infiltration in mice. Sci. Rep. *7*, 597. https://doi.org/10.1038/s41598-017-00721-8.

Zanoni, I., Ostuni, R., Capuano, G., Collini, M., Caccia, M., Ronchi, A.E., Rocchetti, M., Mingozzi, F., Foti, M., Chirico, G., et al. (2009). CD14 regulates the dendritic cell life cycle after LPS exposure through NFAT activation. Nature *460*, 264–268. https://doi.org/10.1038/nature08118.

Zhao, R., Liang, D., and Sun, D. (2016). Blockade of extracellular ATP effect by oxidized ATP effectively mitigated induced mouse experimental autoimmune uveitis (EAU). PLoS One *11*, e0155953. https://doi.org/10.1371/journal.pone.0155953.

Zitvogel, L., Apetoh, L., Ghiringhelli, F., and Kroemer, G. (2008). Immunological aspects of cancer chemotherapy. Nat. Rev. Immunol. *8*, 59–73. https://doi.org/10.1038/nri2216.

iScience, Volume *24*

Supplemental information

Immunogenic tumor cell death promotes dendritic cell migration and inhibits tumor growth via enhanced T cell immunity

Taiki Moriya, Kurumi Kitagawa, Yuuki Hayakawa, Hiroaki Hemmi, Tsuneyasu Kaisho, Satoshi Ueha, Ryoyo Ikebuchi, Ippei Yasuda, Yasutaka Nakanishi, Tetsuya Honda, Koji Matsushima, Kenji Kabashima, Mizuki Ueda, Yutaka Kusumoto, Tatyana Chtanova, and Michio Tomura

Figure S1; related to Figure 1
DT-induced cell death enhances expression and release of DAMPs molecules.

Figure S2; related to Figure 1
Gating strategies for cells in tumors.

Figure S3; related to Figure 2
Analysis of dynamics of tumor infiltrating myeloid cells in MC38-TfROVA-DTRs inoculated KikGR mice.

Figure S4; related to Figure 3
Gating strategy and proportions of migratory DC subsets in dLNs.

Figure S5; related to Figure 3
Immunogenic tumor cell death enhances Ti-DC migration to dLNs.

Figure S6; related to Figure 4
Enhanced Ti-DC migration induced by immunogenic tumor cell death is inhibited by blocking of ATP-P2X7R, HMGB1-TLR4, and G*ai* signaling and S1P-S1PR1 pathways.

Figure S7; related to Figure 6
Tumor cell death induction does not increase expression levels of CD80, CD86, and H-2K^{b} on KikGR-Red CD103^{+} Ti-DCs in dLNs.

Figure S8; related to Figure 7

Table S1; related to Methods
Antibodies for Flow cytometry

Transparent Methods

Supplemental References

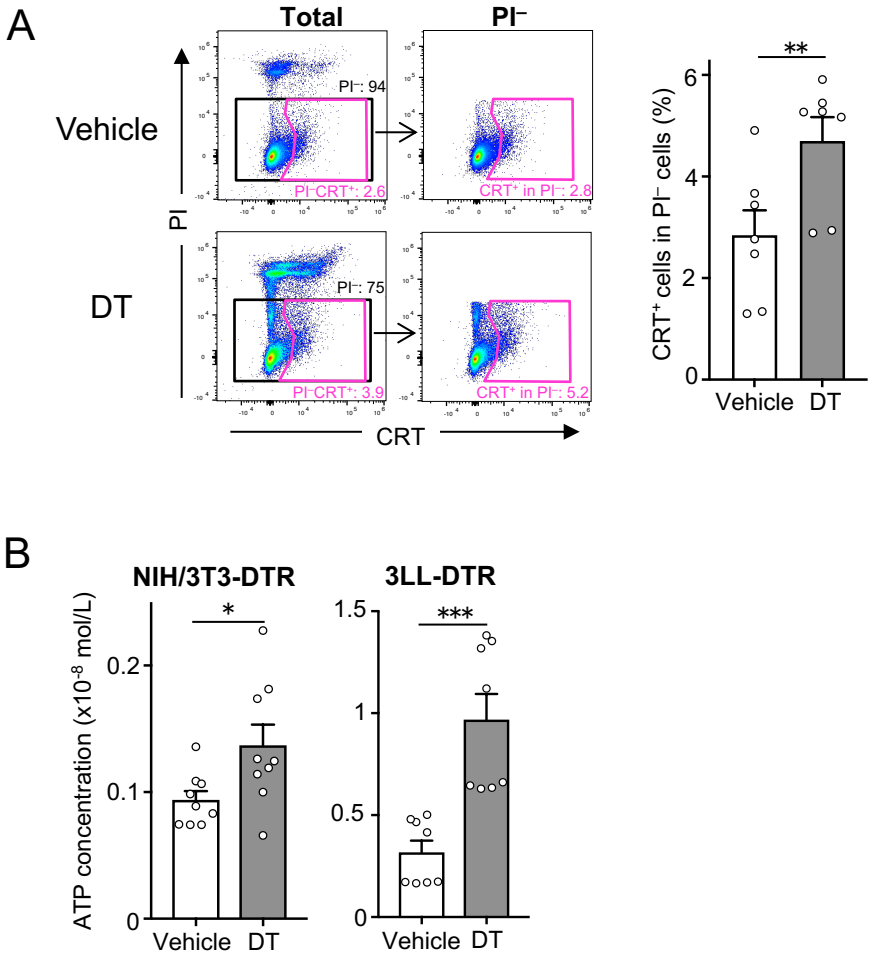

Figure S1; related to Figure 1
DT-induced cell death enhances expression and release of DAMPs molecules.
(A) MC38/TfROVA-DTRs cells 18 hours after vehicle or DT treatment. Gating strategy (left) and proportion (right) of CRT^+ cells in PI^- cell. Numbers in dot plots indicate frequencies of gated population (%) of parent population. Bar graph shows means ± SEM of pooled data from two independent experiments (n=7). $^{**}p<0.01$ (Mann-Whitney U test). (B) ATP concentration in culture supplement of NIH/3T3-DTR and 3LL-DTR cells 12 hours after vehicle or DT treatment. Bar graphs show means ± SEM of pooled data from two independent experiments (n=9). $^{*}P<0.05$, $^{***}p<0.001$ (Mann-Whitney U test).

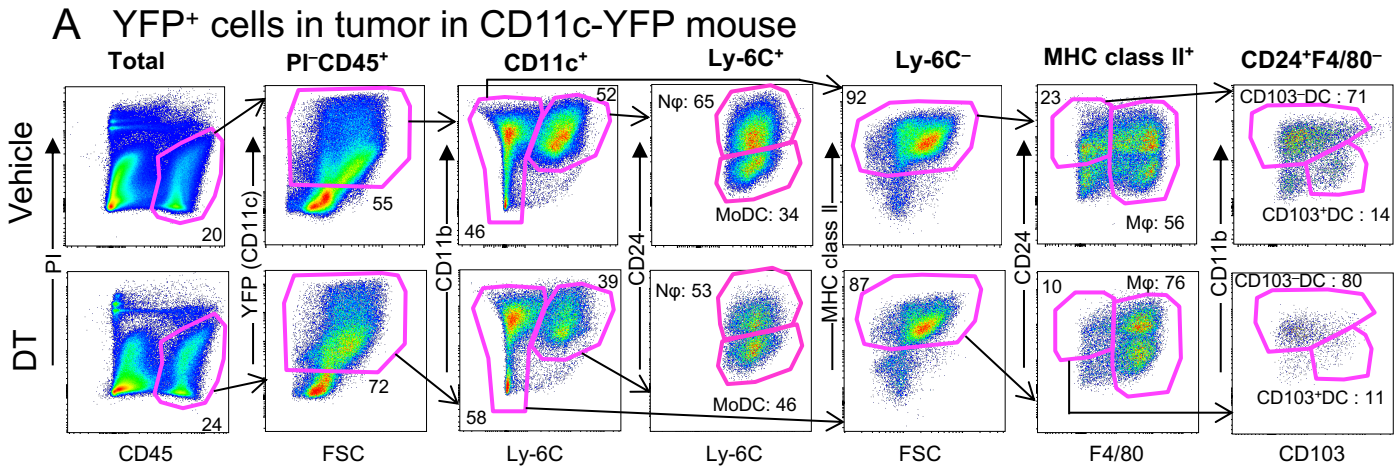

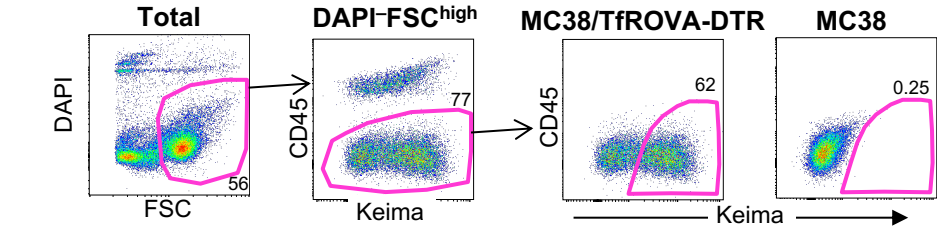

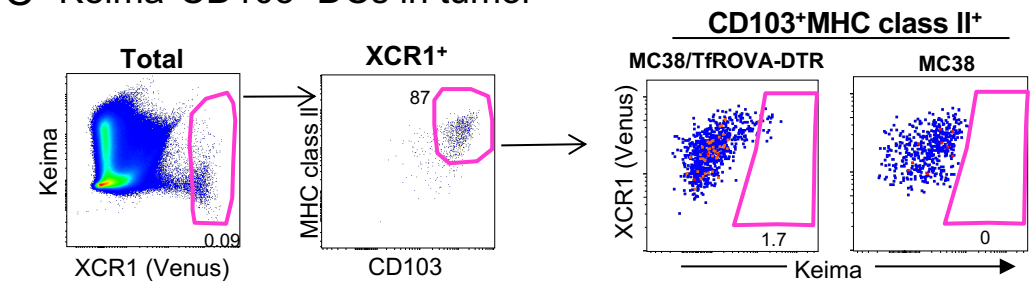

Figure S2; related to Figure 1
Gating strategies for cells in tumors.
(A) Gating strategy for analysis of YFP$^+$ cells in MC38-TfROVA-DTR tumors in CD11c-YFP mice 24 hours after vehicle or DT treatment. (B) Gating strategy for Keima$^+$ live tumor cells in MC38-TfROVA-DTR cells (left) and MC38 cells (right) inoculated mice. (C) Gating strategy for Keima$^+$ Venus$^+$ CD103$^+$ DCs in MC38-TfROVA-DTR cells (left) and MC38 cells (right) inoculated XCR1-Venus mice. Numbers in dot plots indicate frequencies of gated population (%) of parent population.

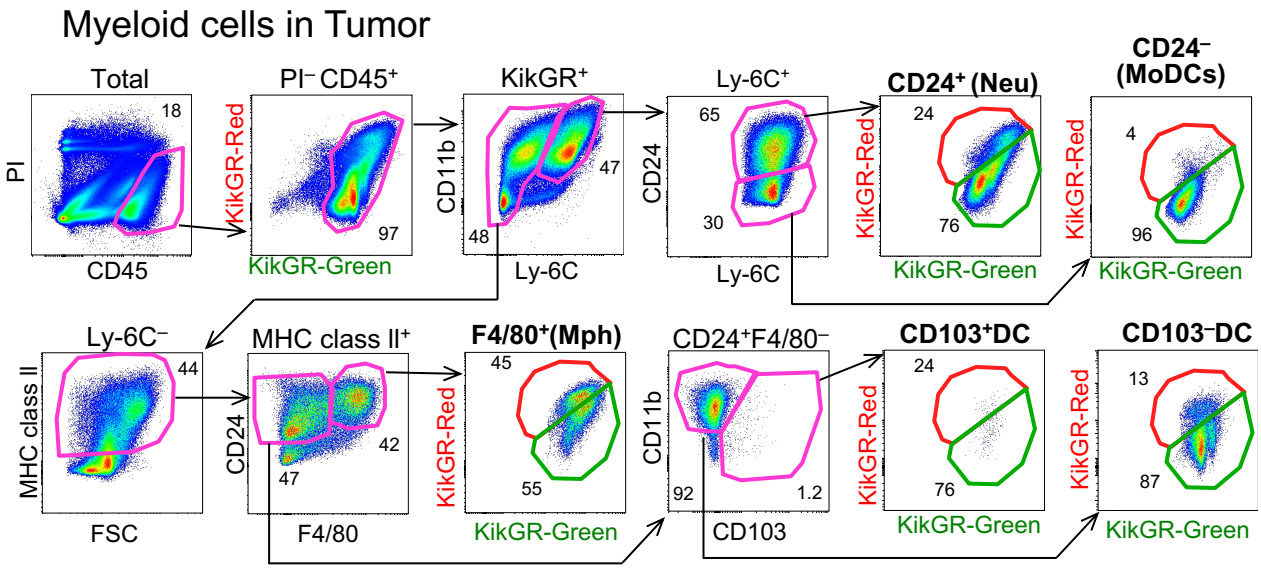

Figure S3; related to Figure 2
Analysis of dynamics of tumor infiltrating myeloid cells in MC38-TfROVA-DTRs inoculated KikGR mice.
Gating strategy for myeloid cells in MC38-TfROVA-DTR tumors inoculated in KikGR mice and photoconverted 24 hours prior to analysis. Numbers in dot plots indicate frequencies of gated population as a % of parent population.

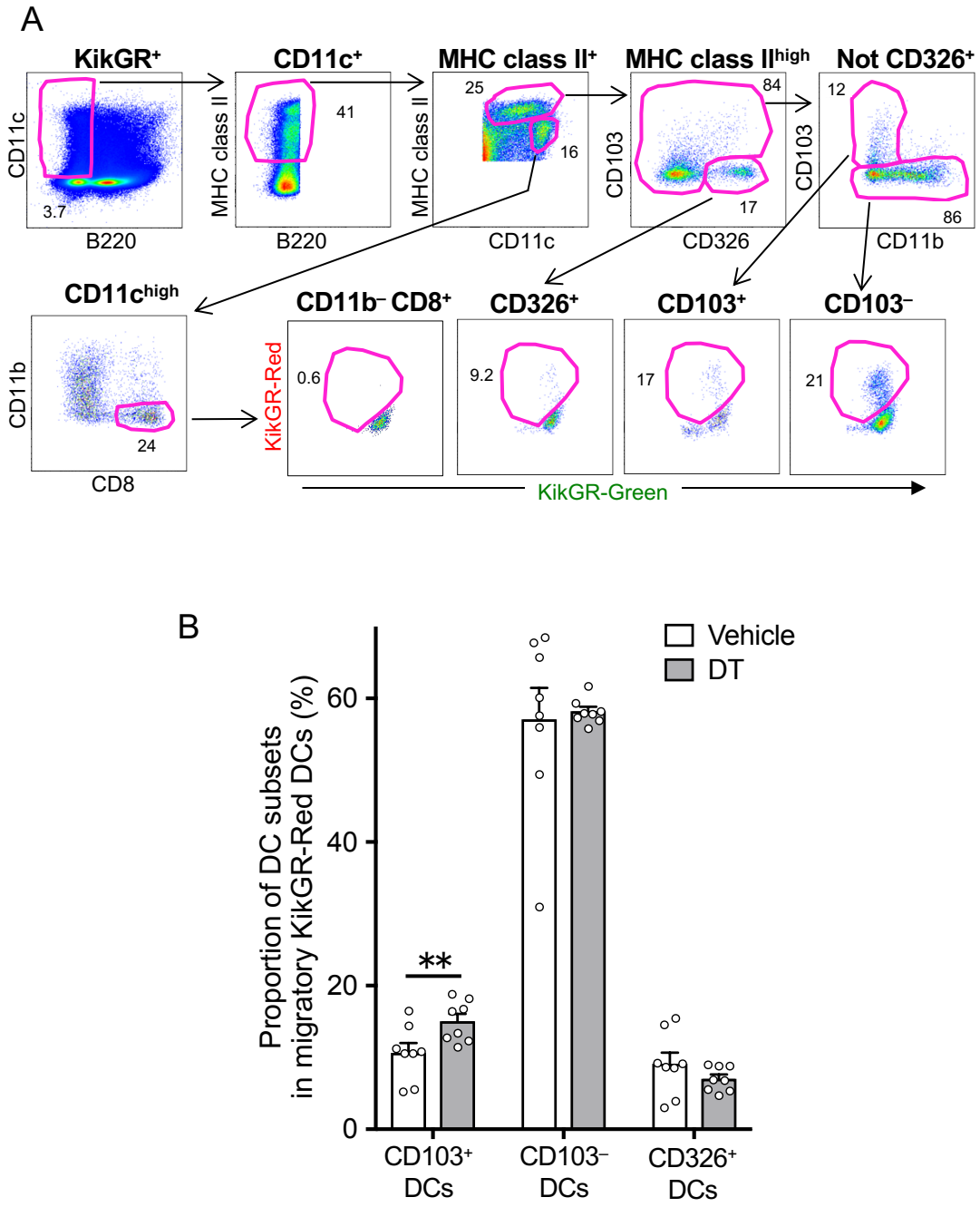

Figure S4; related to Figure 3
Gating strategy and proportions of migratory DC subsets in dLNs
(A) Gating strategy for DCs in dLNs of MC38-TfROVA-DTR tumors inoculated in KikGR mice 24 hours following photoconversion of tumors. Numbers in dot plots indicate frequencies of gated population (%) of parent population. (B) Proportion of 3 DC subsets in migratory KikGR-Red DCs (%) in dLNs in vehicle or DT treated KikGR mice 24 hours after photoconversion. Bar graph shows means ± SEM of pooled data from four independent experiments (n=8). ** P<0.01, (Mann-Whitney U test).

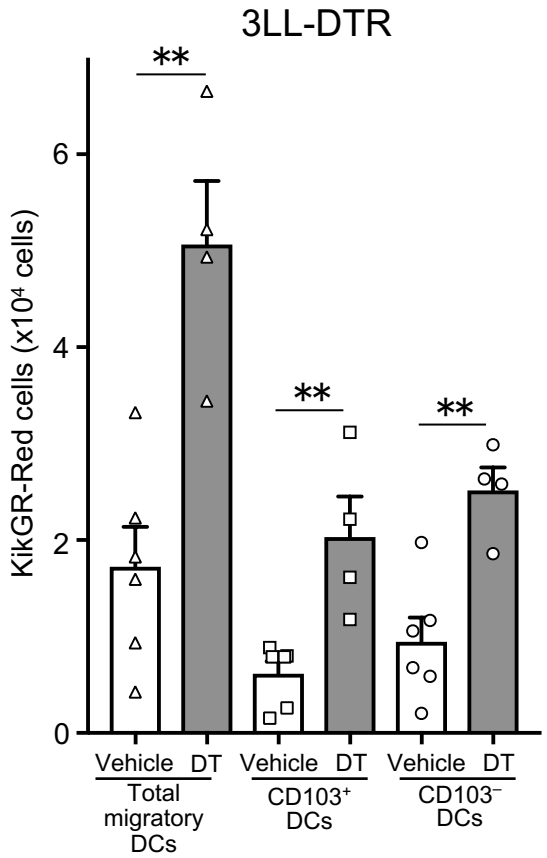

Figure S5; related to Figure 3
Immunogenic tumor cell death enhances Ti-DC migration to dLNs.
KikGR-Red cells in 3 DC subsets in dLNs 24 hours following photoconversion of tumors and vehicle or DT-treated 3LL-DTR tumor in KikGR mice. Bar graphs show means ± SEM of pooled data from two independent experiments (n=4-6). ** P<0.01, (Mann-Whitney U test).

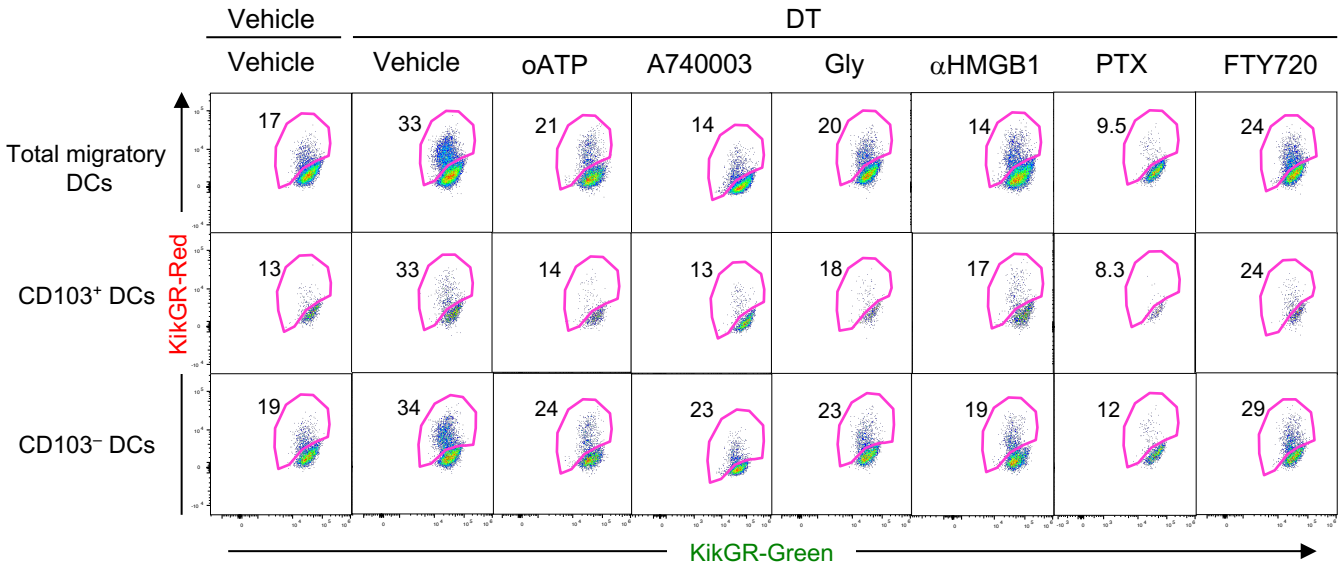

Figure S6; related to Figure 4
Enhanced Ti-DC migration induced by immunogenic tumor cell death is inhibited by blocking of ATP-P2X7R, HMGB1-TLR4, and G*αi* signaling and S1P-S1PR1 pathways.
Representative flow cytometry plots of total migratory DCs, $CD103^+$ DCs, and $CD103^-$ DCs in dLNs of MC38-TfROVA-DTR tumors inoculated in KikGR mice analyzed 24 hours following photoconversion of tumors and indicated treatments. Numbers in dot plots indicate frequencies of gated population (%) of parent population. Data are representative of two to four independent experiments.

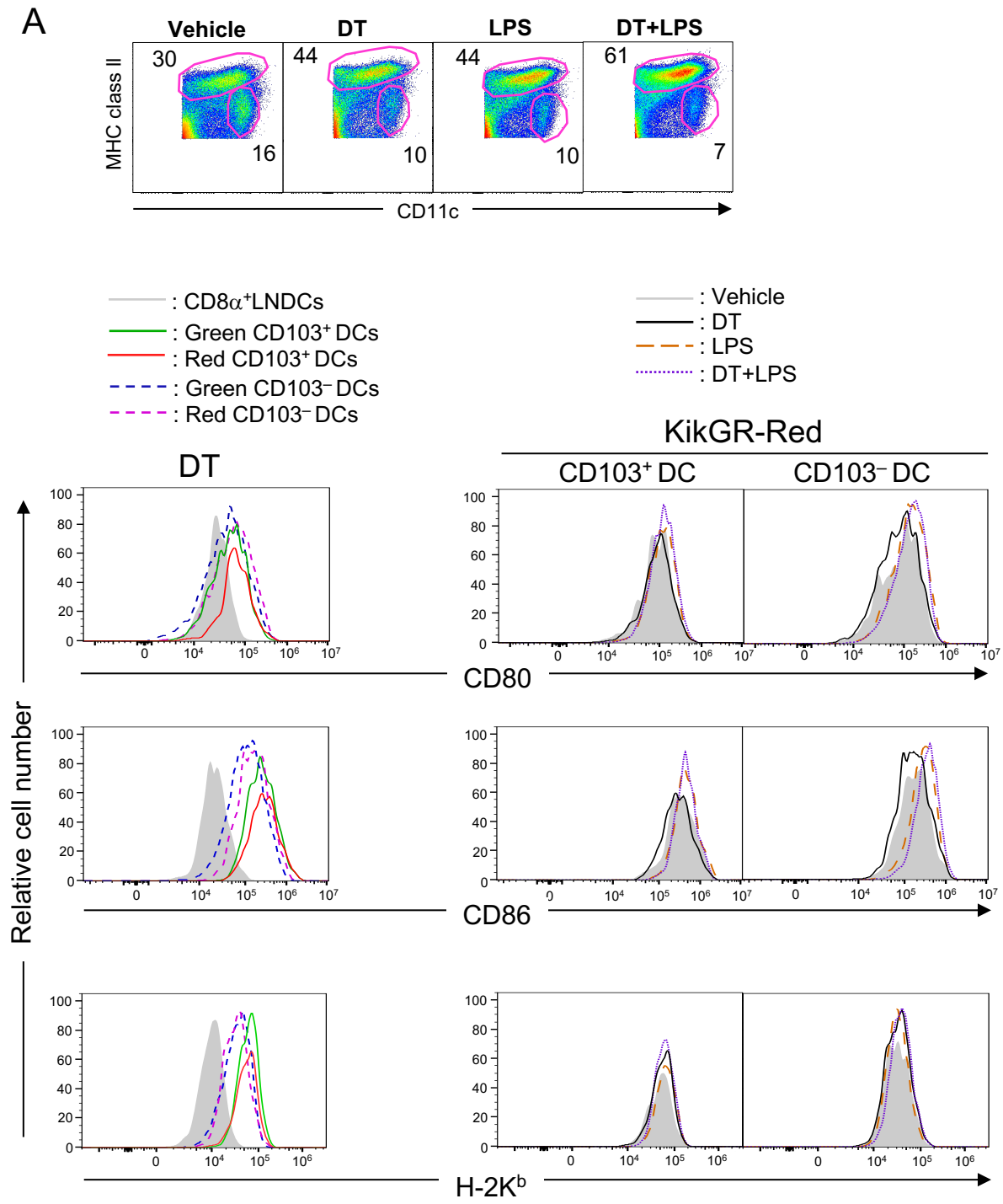
A
Vehicle
DT
LPS
DT+LPS
MHC class II
30
16
44
10
44
10
61
7
CD11c
B
: CD8α+LNDCs
: Green CD103+ DCs
: Red CD103+ DCs
: Green CD103− DCs
: Red CD103− DCs
: Vehicle
: DT
: LPS
: DT+LPS
KikGR-Red
DT
CD103+ DC
CD103− DC
Relative cell number
CD80
CD86
H-2Kb

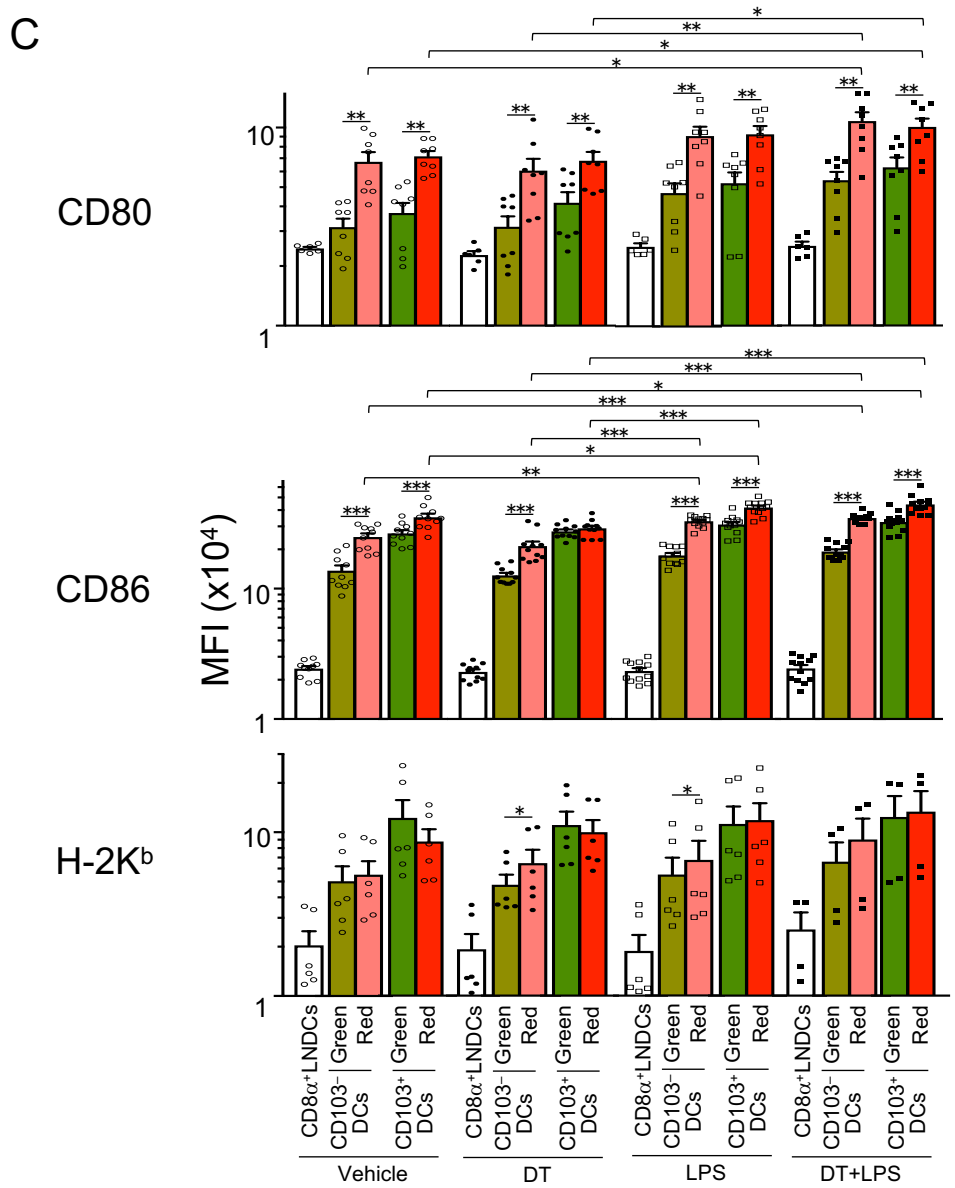

Figure S7; related to Figure 6
Tumor cell death induction does not increase expression levels of CD80, CD86, and H-2K^b on KikGR-Red CD103$^+$ Ti-DCs in dLNs.
(A) Representative flow cytometry plots of migratory DCs and LNDCs in dLN of tumor bearing KikGR mice 24 hours following photoconversion of tumors and vehicle, DT and/or LPS treatments. Numbers in dot plots indicate frequencies of gated population (%) of parent population. Data are representative of at least nine independent experiments. (B) Representative histogram plots of CD80, CD86, and H-2K^b expression in CD8α$^+$ LNDC, KikGR-Green and KikGR-Red CD103$^+$ and CD103$^-$ DCs in dLNs from DT treated KikGR mice bearing tumors consisting of MC38-TfROVA-DTR and MC38 cells (3:7 ratio) 24 hours after photoconversion (left) and in KikGR-Red CD103$^+$ and CD103$^-$ DCs in dLNs from vehicle, DT and/or LPS treated KikGR mice 24 hours after photoconversion (right). Data are representative of at least two independent experiments. (C) MFI values for CD80, CD86 and H-2K^b in each DC subset. Bar graphs show means ± SEM of pooled data from at least two independent experiments (n=4-11). Statistical comparisons were performed using Wilcoxon matched-pairs signed rank test (comparison between KikGR-Green and KikGR-Red cells in each DC subset, *$p < 0.05$, **$p < 0.01$, ***$p < 0.001$) or one-way ANOVA with Kruskal-Wallis test with Dunn's comparisons test (comparison among 4 treatments for the same DC subset, *$p < 0.05$, **$p < 0.01$, ***$p < 0.001$).

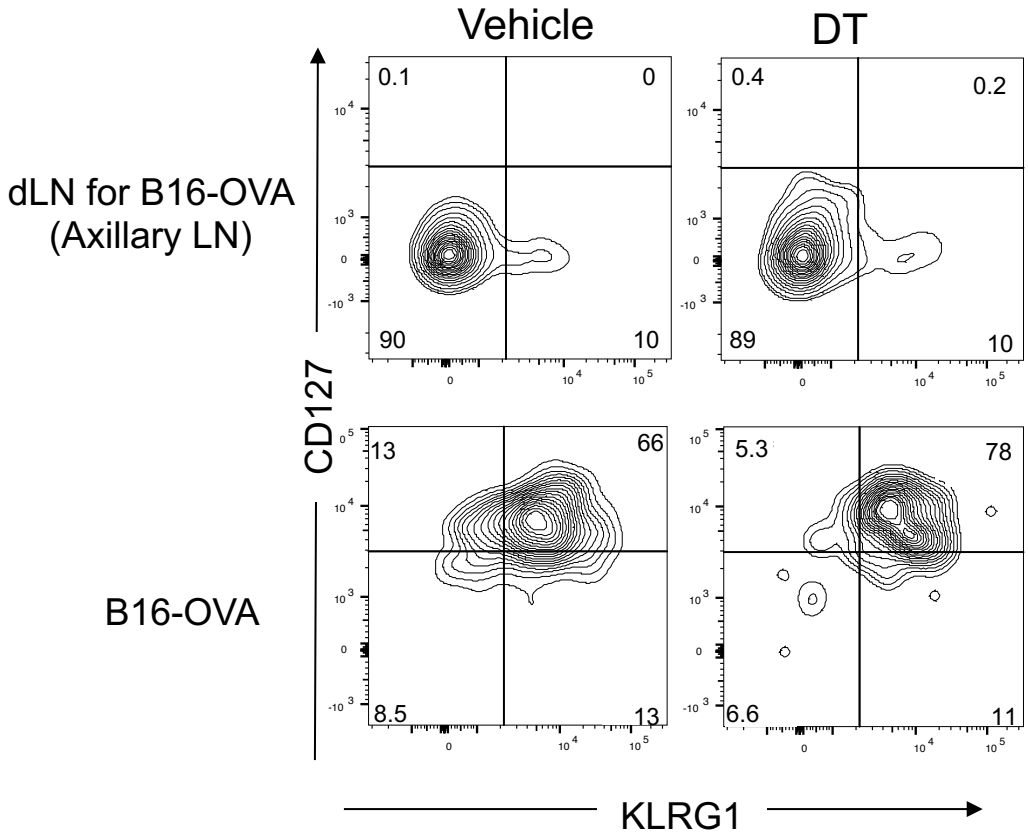

Figure S8; related to Figure 7
Representative flow cytometry plots of OVA-specific $CD8^+$ T cells in dLNs for B16-OVA from vehicle or DT treated tumor bearing mice 2 days after tumor cell death induction. Data are representative of two independent experiments.

Table S1; related to Methods
Antibodies for flow cytometry

Antibody	Clone
CD4	RM4-5
CD5	53-7.3
CD8α	53-6.7
CD11b	M1/70
CD11c	N418
CD19	6D5
CD24	M1/69
CD44	1M7
CD45	30-F11
CD45R/B220	RA3-6B2
CD45.1	A20
CD45.2	104
CD49b/Pan-NK cells	DX5
CD62L	MEL-14
CD69	H1.2F3
CD80	16-10A1
CD86	GL1
CD90.2	53-2.1
CD103	2E7
CD107a	1D4B
CD127	A7R34
CD197 (CCR7)	4B12
CD279 (PD1)	RMP1-30
CD326	G8.8
I-A/I-E	M5/114. 15. 2
H-2K^{b}	AF6-88.5
F4/80	BM8
Ly-6C	HK1.4
TER-119	TER-119
Calreticulin	EPR3924
KLRG1	2F1/KLRG1
TCR-Vα2	B20.1

Transparent Methods

Mice

Knock-in mice carrying KikGR cDNA under the CAG promoter (KikGR mice) were made previously (Tomura et al., 2014). XCR1-DTR mice and XCR1-Venus mice were generated as described previously (Yamazaki et al., 2013). CD11c-YFP mice were kindly provided by Prof. Michel C. Nussenzweig (Lindquist et al., 2004). OT-I transgenic mice (Tg) expressing a TCR specific for OVA in the context of H-2K^{b} (Hogquist et al., 1994) were obtained from Taconic Inc. C57BL/6 mice were purchased from Japan SLC Inc. These mice were bred in specific pathogen–free facilities at Osaka Ohtani University. All experimental procedures were approved by the Institutional Animal Care and Use Committee of Osaka-Ohtani University Faculty of Pharmacy.

Cell lines

The colon adenocarcinoma cell line MC38 (Spiess et al., 1987) was obtained from Shunsuke Chikuma (Kyoto University). The fragment encoding Nuc-tdKeima with NheI and SphI sites was cloned from the pdKeima-NLS3/MC1 vector (Kogure et al., 2006), kind gift from Atsushi Miyawaki (Brain Science Institute, RIKEN). The fragment encoding IRES2 with SphI and BstXI sites was cloned from CSII-CMV-MCS-IRES2-Venus vector kindly provided by Dr Hiroyuki Miyoshi (BioResource center, RIKEN). The TfROVA fragment encoding a fusion protein consisting of the transmembrane domain of the transferrin receptor and OVA (149-385) with BstXI and XbaI sites was cloned from the pIRES puro2-TfrOVA vector (Teasdale et al., 1992). The fragments encoding Nuc-tdKeima with NheI and SphI sites, IRES2 with SphI and BstXI sites, and TfROVA with BstXI and XbaI sites were ligated and cloned into the NheI and XbaI digestion site of CSII-CMV-MCS-IRES2-Venus by blunt end ligation (CSII-CMV-Nuc-tdKeima-IRES2-TfROVA). pTRECK6 and pCAGTR6-GFP was kindly provided by Dr. Kenji Kohno (Nara Institute of Science and Technology)(Furukawa et al., 2006; Saito et al., 2001). The fragment of human HB-EGF (DTR) complementary DNA (cDNA) was isolated from pTRECK6 by EcoRI digestion, and cloned into EcoRI site of pCAGTR6-GFP, and the fragment of CAG-HB-EGF was isolated by SalI and HindIII digestion. pBS-Lox-PGK-gb2-Hyg-Lox sequence was isolated from pBS-Lox-PGK-gb2-Hyg-Lox vector (Gene Bridges) by NotI and XhoI

digestion, and cloned into the same digestion site in pBluescript II-SK+ vector, and then the fragment of CAG-HB-EGF was cloned into SalI and HindIII digestion site, and fragment of pBS-Lox-Hyg-CAG-HB-EGF was obtained by XhoI and NotI digestion. CSII-CMV-Nuc-tdKeima-IRES2-TfROVA vector was digested by SacII, and XhoI and NotI digestion sites were introduced in SacII digestion site of CSII- CMV-Nuc-tdKeima-IRES2-TfROVA by using synthetic oligomers CSII-S: CTGTATCAAGCACATCGCAACCAACGCCG and CSII-AS: AGCAGGCCGCGGGCGGCCGCTTCAGTTC. And then, obtained vector was digested by XhoI and NotI and the fragment of pBS-Lox-Hyg-CAG-HB-EGF was cloned (pCSII-CMV-Nuc-tdKeima-IRES2-TfrOVA-Lox-PGK-Hyg-Lox-CAG-HB-EGF). To obtain MC38/TfROVA-DTRs and MC38/TfROVA, linearized pCSII-CMV-Nuc-tdKeima-IRES2-TfrOVA-Lox-PGK-Hyg-Lox-CAG-HB-EGF or pCSII- CMV-Nuc-tdKeima-IRES2-TfROVA was transfected to MC38 with Amaxa (Lonza), and transfectants were selected by zeocin, respectively and Keima^{+} cells were sorted and used for experiments. B16-OVA was kindly gifted by Dr. Masakazu Hattori (Kyoto University). pCAGTR6-GFP was transfected into 3LL and NIH/3T3 using Lipofectamine 3000 (Thermo Fisher Scientific K. K.) to establish 3LL and NIH/3T3 expressing DTR (3LL-DTR, NIH/3T3-DTR). MC38, B16, 3LL-DTR, NIH/3T3-DTR, MC38/TfROVA-DTR and B16-OVA cell lines were maintained in culture medium consisted of Roswell Park Memorial Institute-1640 medium (RPMI; Sigma) supplemented with 10% (v/v) heat-inactivated bovine calf serum (BCS; Hyclone), 1% (v/v) Penicillin-Streptomycin-Glutamine mixed solution (NACALAI TESQUE, INC.), 10mmol/L HEPES Buffer Solution (NACALAI TESQUE, INC.) and 1% (v/v) non-essential amino acids solution (NACALAI TESQUE, INC.). Tumor cell lines were kept at 37˚C in a humidified atmosphere of 95% air and 5% CO2 until use. Culture medium was replaced every 2 or 3 days.

Inoculation of tumor cell lines and evaluation of tumor growth

MC38/TfROVA-DTRs or 3LL-DTR were harvested and single-cell suspensions of 2×10^6 / 100 μL were intradermally inoculated into abdominal skin. For partial tumor cell death induction experiments, mixture of 1.4×10^6 of MC38/TfROVA-DTR cells and 0.6×10^6 of MC38 cells in 100 μL was intradermally inoculated into abdominal skin. Single-cell suspensions of 5×10^5 of B16-OVA or B16 in 100 μL were injected subcutaneously into the

flank. Tumor volumes were determined by caliper measurements and calculated using the formula: V=4⁄3*π*width/2*depth/2*height/2.

Photoconversion and surgical procedures

Tumor photoconversion was performed 5 days after tumor inoculation, as described previously (Nakanishi et al., 2017; Tomura et al., 2014). Briefly, KikGR mice were anesthetized with isoflurane (DS Pharma Animal Health) and luminal side of tumors was subjected to 120 seconds exposures to violet light (436 nm, 200 mW/cm^2) using SP500 spot UV curing equipment with a 436 nm bandpass filter (USHIO). During photoconversion, skin around tumors was protected from light with aluminum foil. After photoconversion, the abdominal wall was closed by suture. To keep exposed tissues moist during exposure to light, warmed phosphate buffered saline (PBS) was applied to region of photoconversion.

Cell isolation

Cell suspensions from tumors were prepared by enzymatic digestion. Tumors were finely dissected in RPMI 1640-medium (Sigma-Aldrich) containing 300 U/mL of collagenase from C.Histolyticum (Sigma-Aldrich), and 1 mg/mL of dispase II (Roche). After mincing with scissors, tumors were incubated in the same solution for 30 min at 37 ° C. After adding 2000 U/mL of DNase I (Calbiochem), cell suspensions were incubated for 15 min at 37 ° C, and filtered through a cell strainer. Preparation of cell suspensions from the LNs by enzymatic digestion was described previously (Tomura et al., 2014). Briefly, cell in LNs were extruded into RPMI 1640-medium containing 100 U/mL of collagenase type IV (Worthington) and 2000 U/mL of DNase I and incubated for 15 min at 37° C. After adding 0.5 M EDTA, cell suspensions were filtered through a cell strainer.

***In vitro* T cell proliferation assay**

Five days after tumor inoculation in KikGR mice, tumors were photoconverted. Twenty-four hours later, CD11c-positive cells in dLNs of tumor bearing KikGR mice were positively sorted using anti-CD11c magnetic microbeads (Miltenyi Biotec). Sorted cells were stained with Allophycocyanin (APC)-conjugated anti-mouse CD11c monoclonal antibody (mAb) and Alexa Fluor 700-conjugated anti-mouse I-A/I-E mAb, and KikGR-Red

and KikGR-Green cells in $CD11c^+$ MHC class II^{high} migratory DCs and KikGR-Green cells in $CD11c^{high}$ MHC class II^{int} LNDCs were sorted by SH800 (SONY). Mixture of LN and spleen cells from OT-I Tg mice were stained with biotinylated-CD4, CD11b, CD11c, CD19, CD49b, and TER-119 mAbs and negatively sorted using anti-biotin MACS beads (Miltenyi Biotec). Purity of $CD8^+$ TCR-$V\alpha2^+$ cells was >95 %. $CD8^+$ TCR-$V\alpha2^+$ cells (2×10^5 cells) were labeled with CellTrace Violet (Life Technologies) according to the manufacturer's protocol and co-cultured with sorted $CD11c^+$ MHC class II^{high} migratory KikGR-Red, KikGR-Green DCs or $CD11c^{high}$ MHC class II^{int} LNDCs (3×10^4 cells) for 72 hours in 96 well plate with in 2-Mercaptoethamnol containing RPMI-1640 medium. After three days of culture, cells were harvested and stained with PE/Cy7-conjugated anti-CD8 mAb, and APC-conjugated anti- TCR-$V\alpha2^+$ mAb and analyzed by flow cytometry. $CD8^+$ TCR-$V\alpha2^+$ T cell proliferation was evaluated by dilution of CellTrace Violet.

OT-I T-cell adoptive transfer and proliferation assay

Five days after tumor inoculation, mice were treated with DT and/or LPS, and twenty-four hours later, 1×10^6 of $CD8^+$ TCR-$V\alpha2^+$ CellTrace Violet labeled OT-I T cells were transferred intravenously. Forty-five hours after transfer, $CD8^+$ TCR-$V\alpha2^+$ T cell proliferation was evaluated by dilution of CellTrace Violet.

Microscopy and histology

Fluorescence images of tumors were captured with two-photon microscopy (A1, Nikon) or inverted microscope (ECULIPSE Ti-E, Nikon). For tumor imaging with inverted microscope, frozen sections of tumors were made. Five days after tumor inoculation, tumor bearing CD11c-YFP mice were treated with DT or vehicle and 24 hours later, tumors were dissected. After 24h fixation with 4% paraformaldehyde (Wako Chemicals), tumors were placed in 30% sucrose as a cryoprotectant. Frozen tissues were cut into 10 or 20 μm thick sections using a cryostat (CM1850, Leica) and observed with a fluorescence microscope.

Antibodies and Flow cytometry

Fluorochrome-conjugated or biotinylated mAbs and fluorochrome-conjugated avidin were obtained from BD Bioscience, eBioscience, Medical and Biological Laboratories co., ltd (MBL), Abcam or BioLegend. Details are listed in Supplementary Table 1. For flow cytometric analysis, cells were washed with Dulbecco's PBS containing 2% FCS and 0.02% sodium azide. Next, cells were incubated with 2.4G2 hybridoma culture supernatant to block Fc binding, then stained with biotinylated mAbs followed by Brilliant Violet 421-conjugated streptavidin or fluorochrome-labeled mAbs for 15 minutes at 4 ºC. For detection of OVA-specific TCR-bearing cells, cells were stained with phycoerythrin-conjugated H-2K^{b} OVA tetramer-SIINFEKL (MBL) for 30 minutes at room temperature (22-24 ºC) followed by staining with fluorochrome-labeled mAbs. Dead cells were labeled with Propidium Iodide (Wako) or 7-amino-actinomycin D just before flow cytometry analysis using SP6800 (SONY). Flow cytometry data were analyzed using FlowJo software (Tree Star). The number of cells per gram of tumor was calculated by dividing the number of cells obtained from flow cytometric analysis by the weight of the tumor used for the analysis. The number of cells in each cell subset in the lymph node was calculated by multiplying the total number of cells by the frequency of each cell subset obtained by flow cytometric analysis.

Reagents and treatment

One microgram of DT (Sigma-Aldrich) in PBS was injected intraperitoneally into tumor bearing mice 5 days after tumor inoculation. In some experiments, tumor bearing mice were intratumorally treated with 250 ng of LPS (Sigma-Aldrich) 5 days after tumor inoculation. Three hundred μg of oATP, 1 μg of A740003 (ChemScene), 50 μg of aHMGB1 mAb (Biolegend), 5 mg of glycyrrhizin dipotassium salt hydrate (Tokyo Chemical Industry), 100 μg of FTY720 (Cayman Chemical), or 500 ng of PTX (Wako) were injected intraperitoneally at the same time as DT treatment.

CRT expression assay

Single-cell suspensions of MC38/TfROVA-DTR cells (1.5×10^5 cells / 500 μL in serum-free media) were seeded into a 24-well dish and incubated for 3 hours, then 500 ng of DT was added. Eighteen hours later, cells were harvested and stained with anti-CRT mAbs and analyzed by flow cytometry.

HMGB1 and ATP release assay

Single-cell suspensions of MC38/TfROVA-DTR, 3LL-DTR or NIH/3T3-DTR cells (1.5×10^5 / 500 μL in serum-free media) were seeded into a 24-well dish and incubated for 3 hours, then 500 ng of DT was added. Twelve hours later, culture supernatants were harvested. HMGB1 and ATP concentrations in supernatants were measured by HMGB1 ELISA Kit (Arigo Biolaboratories Corp) and the luciferin-based ENLITEN ATP Assay (Promega, Madison, WI, USA), respectively.

Statistical analysis

Data were tested by Mann-Whitney's U test, one-way ANOVA with Holm-Sidak's multiple comparisons test, Kruskal-Wallis test with Dunn's comparisons test, two-way ANOVA with Sidak's multiple comparisons test, or Wilcoxon matched-pairs signed rank test, which were selected depending on the comparison group and data distribution. All tests were done using GraphPad Prism version 7.0 (GraphPad Software). Data in bar graphs represent means ± SEM. P-values of less than 0.05 were considered to be statistically significant and labeled: *, $P < 0.05$; **, $P < 0.01$; or ***, $P < 0.001$.

Supplemental References

Furukawa, N., Saito, M., Hakoshima, T., Kohno, K., 2006. A diphtheria toxin receptor deficient in epidermal growth factor-like biological activity. J. Biochem. 140, 831–841. https://doi.org/10.1093/jb/mvj216

Hogquist, K.A., Jameson, S.C., Heath, W.R., Howard, J.L., Bevan, M.J., Carbone, F.R., 1994. T cell receptor antagonist peptides induce positive selection. Cell 76, 17–27. https://doi.org/10.1016/0092-8674(94)90169-4

Kogure, T., Karasawa, S., Araki, T., Saito, K., Kinjo, M., Miyawaki, A., 2006. A fluorescent variant of a protein from the stony coral Montipora facilitates dual-color single-laser fluorescence cross-correlation spectroscopy. Nat. Biotechnol. 24, 577–581. https://doi.org/10.1038/nbt1207

Lindquist, R.L., Shakhar, G., Dudziak, D., Wardemann, H., Eisenreich, T., Dustin, M.L., Nussenzweig, M.C., 2004. Visualizing dendritic cell networks in vivo. Nat. Immunol. 5, 1243–1250. https://doi.org/10.1038/ni1139

Nakanishi, Y., Ikebuchi, R., Chtanova, T., Kusumoto, Y., Okuyama, H., Moriya, T., Honda, T., Kabashima, K., Watanabe, T., Sakai, Y., Tomura, M., 2017. Regulatory T cells with superior immunosuppressive capacity emigrate from the inflamed colon to draining lymph nodes. Mucosal Immunol. https://doi.org/10.1038/mi.2017.64

Saito, M., Iwawaki, T., Taya, C., Yonekawa, H., Noda, M., Inui, Y., Mekada, E., Kimata, Y., Tsuru, A., Kohno, K., 2001. Diphtheria toxin receptor-mediated conditional and targeted cell ablation in transgenic mice. Nat. Biotechnol. 19, 746–750. https://doi.org/10.1038/90795

Spiess, P.J., Yang, J.C., Rosenberg, S.A., 1987. In vivo antitumor activity of tumor-infiltrating lymphocytes expanded in recombinant interleukin-2. J. Natl. Cancer Inst. 79, 1067–1075.

Teasdale, R.D., D'Agostaro, G., Gleeson, P.A., 1992. The signal for golgi retention of bovine β1,4-galactosyltransferase is in the transmembrane domain. J. Biol. Chem. 267, 4084–4096.

Tomura, M., Hata, A., Matsuoka, S., Shand, F.H.W., Nakanishi, Y., Ikebuchi, R., Ueha, S., Tsutsui, H., Inaba, K., Matsushima, K., Miyawaki, A., Kabashima, K., Watanabe, T., Kanagawa, O., 2014. Tracking and quantification of dendritic cell migration and antigen trafficking between the skin and lymph nodes. Sci. Rep. 4, 1–11. https://doi.org/10.1038/srep06030

Yamazaki, C., Sugiyama, M., Ohta, T., Hemmi, H., Hamada, E., Sasaki, I., Fukuda, Y., Yano, T., Nobuoka, M., Hirashima, T., Iizuka, A., Sato, K., Tanaka, T., Hoshino, K., Kaisho, T., 2013. Critical Roles of a Dendritic Cell Subset Expressing a Chemokine Receptor, XCR1. J. Immunol. 190, 6071–6082. https://doi.org/10.4049/jimmunol.1202798